

Review

Overview of the Fundamentals and Applications of Bifacial Photovoltaic Technology: Agrivoltaics and Aquavoltaics

Elmehdi Mouhib ^{1,*}, Leonardo Micheli ², Florencia M. Almonacid ¹ and Eduardo F. Fernández ^{1,*}

¹ Advances in Photovoltaic Technology (AdPVTech), CEA CTEMA, University of Jaén (UJA), 23071 Jaén, Spain

² Department of Astronautical, Electrical and Energy Engineering (DIAEE), Sapienza University of Rome, 00184 Rome, Italy

* Correspondence: emouhib@ujaen.es (E.M.); eduardo.fernandez@ujaen.es (E.F.F.)

Abstract: Bifacial technology is attracting the attention of the photovoltaic community. Although considered premature, research and development activities still need to be carried out to improve bPV performance. In addition, the need for a standard test reference will aid bankability and increase confidence in this technology. This article describes the state of the art of bifacial technology, going through the bPV cell and its difference compared to conventional monofacial cells and listing the different sources of limitations, with an identification of different parameters that characterize the performance of the bifacial. Then, the paper reviews the different modeling methods that allow predicting the performance of bPV systems, and ends with the most important applications, whether for dual use of land to produce energy and food (agrivoltaic) or for placing bPV modules on water bodies instead of on the ground (aquavoltaics), or for vertical use as solar fences, acoustic barriers, or building-integrated photovoltaic modules.

Keywords: bifacial; photovoltaic; BPV modeling; BPV applications; agrivoltaic; aquavoltaic



Citation: Mouhib, E.; Micheli, L.; Almonacid, F.M.; Fernández, E.F. Overview of the Fundamentals and Applications of Bifacial Photovoltaic Technology: Agrivoltaics and Aquavoltaics. *Energies* **2022**, *15*, 8777. <https://doi.org/10.3390/en15238777>

Academic Editor: Antonio Gagliano

Received: 13 October 2022

Accepted: 14 November 2022

Published: 22 November 2022

Publisher's Note: MDPI stays neutral with regard to jurisdictional claims in published maps and institutional affiliations.



Copyright: © 2022 by the authors. Licensee MDPI, Basel, Switzerland. This article is an open access article distributed under the terms and conditions of the Creative Commons Attribution (CC BY) license (<https://creativecommons.org/licenses/by/4.0/>).

1. Introduction

Unlike conventional monofacial cells, bifacial PV (bPV) cells convert solar energy from both sides of the cell into electricity. Therefore, bPV cells make use of the global radiation on the front side and of the mainly-reflected rays coming from the ground to the rear side. Bifacial technology can increase the power density of photovoltaic energy compared to monofacial cells. At the same time, bPV modules lower the relative cost of the surface area of photovoltaic systems, as they take up less space than monofacial ones to provide the same amount of solar power [1].

The research on bifacial PV technology began in 1960 [2]. A few years later, the study of the experimental application of bPV performance was initiated [3,4]. However, this technology has gained significant interest only since the 2010s as can be seen in Figure 1. In that decade, international researchers started working more intensively on these bifacial cells and modules, and companies such as Sanyo Co., Yingli Solar, PVG Solutions, bSolar, etc., have marketed bifacial PV modules with c-Si bifacial photovoltaic cell structures [5,6].

In previous work, the use of bifacial technology showed an increase in energy yield compared to monofacial of up to 30% [7], with an initial cost increment of 5–6 ¢/W which leads to a reasonable rise in production costs [8]. The increase in energy generation depends on different factors, such as the ground reflectivity (albedo), the module clearance, the bifaciality, and the orientation [9]. Additionally, the use of bifacial PV in power plants can be more cost-effective, especially for high albedos, resulting in a lower LCOE (levelized cost of energy) compared to conventional mono PV [10,11], and can decrease the BOS (balance of system) price per watts installed [12]. Since the rays are received from both sides of the cell, a question can be raised about the temperature of the bifacial cell. However, since the convective heat exchange is dominant, the temperature of the bPV and mono PV cells are not far apart at ambient conditions [13].

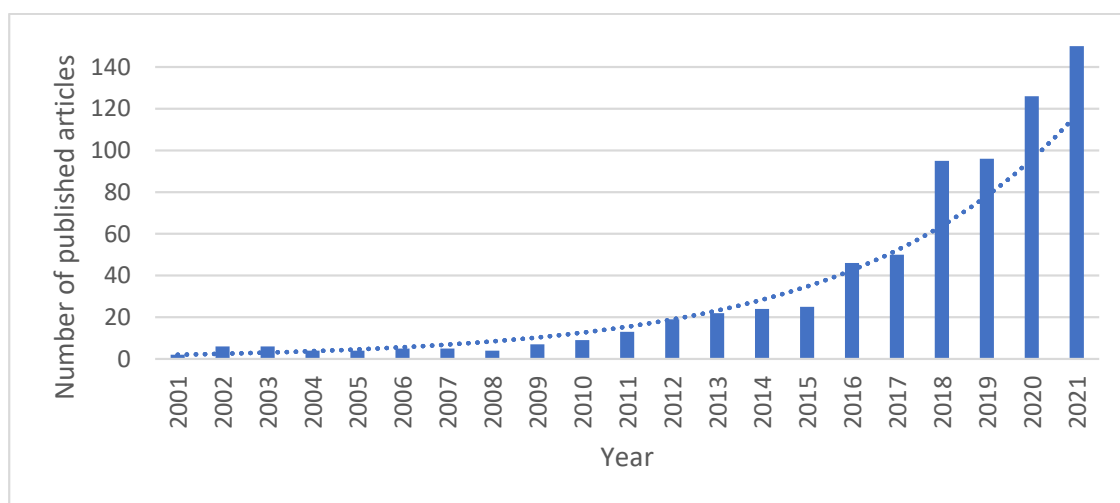


Figure 1. Articles published on bPV technology over the last 20 years with the key word “bifacial photovoltaic” (Source: Scopus).

Bifacial technology is expected to be the major player in the PV global market. The international technology roadmap for PV foresees the market share of PV modules to increase from 20% in 2020 to 70% in 2030. In 2013, a large-scale photovoltaic power plant was built for the first time in the city of Hokuto (Japan), which has a capacity of 1.25 MWp. This plant recorded a gain of 21.9% in the first year compared to a similar-sized mono-PV power plant [14]. So far, the largest bPV power plant under construction is a 900 MWp system with tracking configuration being built by the Saudi company ACWA Power in Dubai [15]. This project will help to accelerate the learning of bPV technology. One of the main ways to improve a solar PV plant is to include a sun tracking system. One would expect that tracking would increase the energy yield also in bPV, as it would maximize the front-side irradiance. However, one question that could be raised is whether maximizing the front direct irradiance with tracking will create significant shading on the ground that could reduce the contribution of reflected irradiance on the ground (albedo). Despite this, two-year tests show that two-axis trackers for bifacial systems produce 14% more electricity in a year compared to monofacial, and at least 35% more than a fixed-tilt system [16]. This suggests dual-axis tracking as an economically attractive solution, especially for northern latitudes.

One of the major challenges of bPV technology is the ability to fully model rear irradiance in different operating conditions. However, two factors can be identified as critical to the acceptability of bifacial photovoltaic devices: formulation of an indoor bifacial photovoltaic performance characterization standard and a full outdoor performance characterization simulation model. The establishment of standards and an accurate modeling methodology will enhance the bankability of bifacial photovoltaic technology. Moreover, the simulation model is able to serve a useful role in the large-scale photovoltaic systems design and implementation, either an optical model to quantify the irradiation received at the front, for example, the isotropic model of Liu and Jordan [17], or the improved version [18]. For rear-side irradiance it is more complex. The common simulation methods are: (I) view factors by simulating the portion of the rays that leave one surface and hit another and (II) ray tracing by following the path of the rays. These two methods will be discussed in this paper in the optical modeling section. Thermal and electrical methods to simulate the bPV cell temperature and electrical performance will also be discussed.

The economic competitiveness of the technology is another challenge that may limit its market expansion. Suitable applications of bifacial technology have been explored, such as agrivoltaics, with simultaneous land use between agriculture and PV modules [19], or building-integrated PV, where bPV modules can replace conventional building materials on the roof, in skylights, on facades, or as acoustic barriers [20]. bPV technology has also been

applied in floating photovoltaics, in which modules are installed on or above water surfaces (lakes, reservoirs, or dams) to produce electricity and, in some cases, aquaculture [21]. Further understanding of the performance of bifacial photovoltaic applications will help validate their relevance. Several articles have reviewed the bifacial technology, but we have seen that detailing the different applications of the bifacial technology can be very useful to complete the knowledge in this field. For this reason, this article will concentrate more on the performance of bPV technology in different applications, such as agrivoltaic, acoustic barriers, and floating PV. The main scope is to review the state-of-the-art of bifacial photovoltaic technology. This article is divided into three parts: fundamentals of bifacial photovoltaic technology and performance parameters, the different modeling methods (optical, electrical and thermal), and the main applications of bPV technology (agrivoltaic, aquavoltaic, and vertical).

2. Bifacial PV Technology

2.1. Bifacial PV Cells

The principle of operation of bifacial bPV technology is the same as that of mono PV technology, namely the photoelectric effect. Photons with energy greater than the band gap transfer their energy to the electron e^- and give rise to electron-hole pairs [22]. The carriers generated nearby the semiconductor's depletion region do not recombine, but rather diffuse toward the substrate and emitter and are attracted by the inner electric field, directing electrons and holes toward the N-type and P-type semiconductors, respectively. Between the front and rear contacts, an electromotive force is created as a result. When the two sides of the photovoltaic cells are connected, electrons move through the external charge. However, differently from monofacial systems, bifacial modules can make use of light hitting both the front and back glass of the bPV cells. Because of their bifacial characteristics, both the front and the rear glasses are covered with anti-reflective (AR) coatings. To improve the irradiation absorption of the bifacial photovoltaic cell, the back contact is fabricated in the form of an open metallization grid, either in Ag or Al metals, which is not the case for the monofacial (Figure 2). The back contact in the monofacial cell is a separate layer covering the entire back of the cell, and this is the structural difference between a mono and a bifacial photovoltaic cell [23].

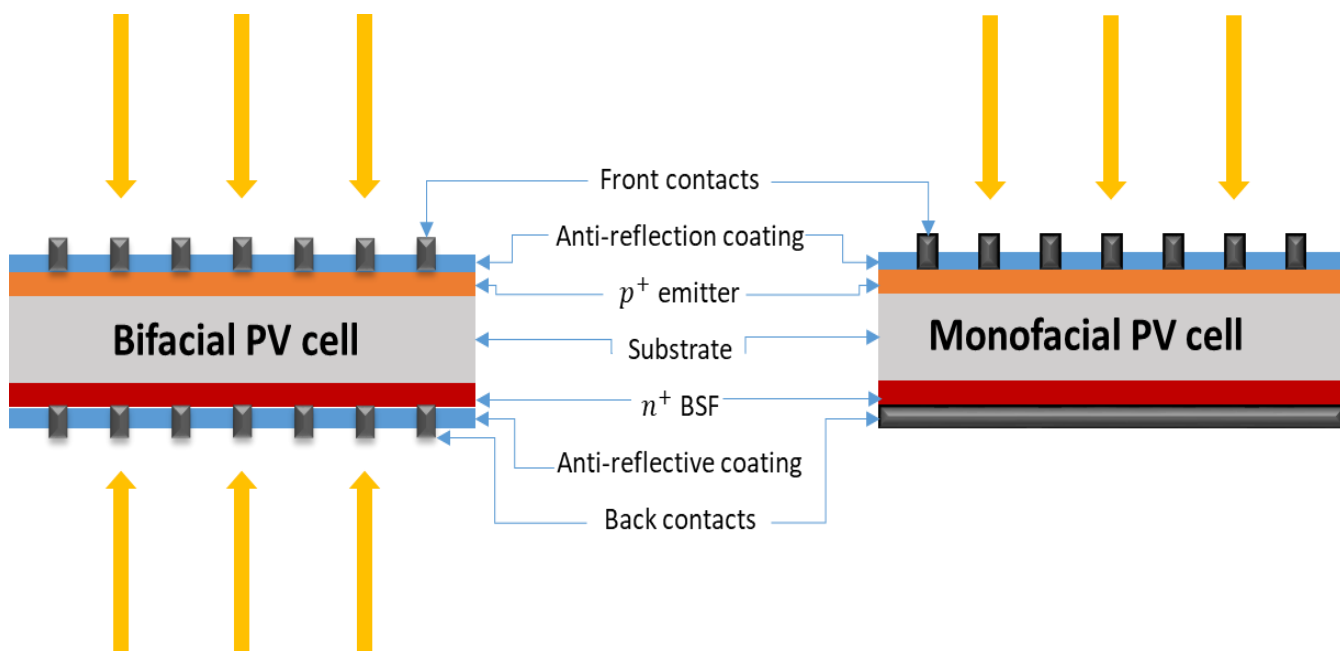
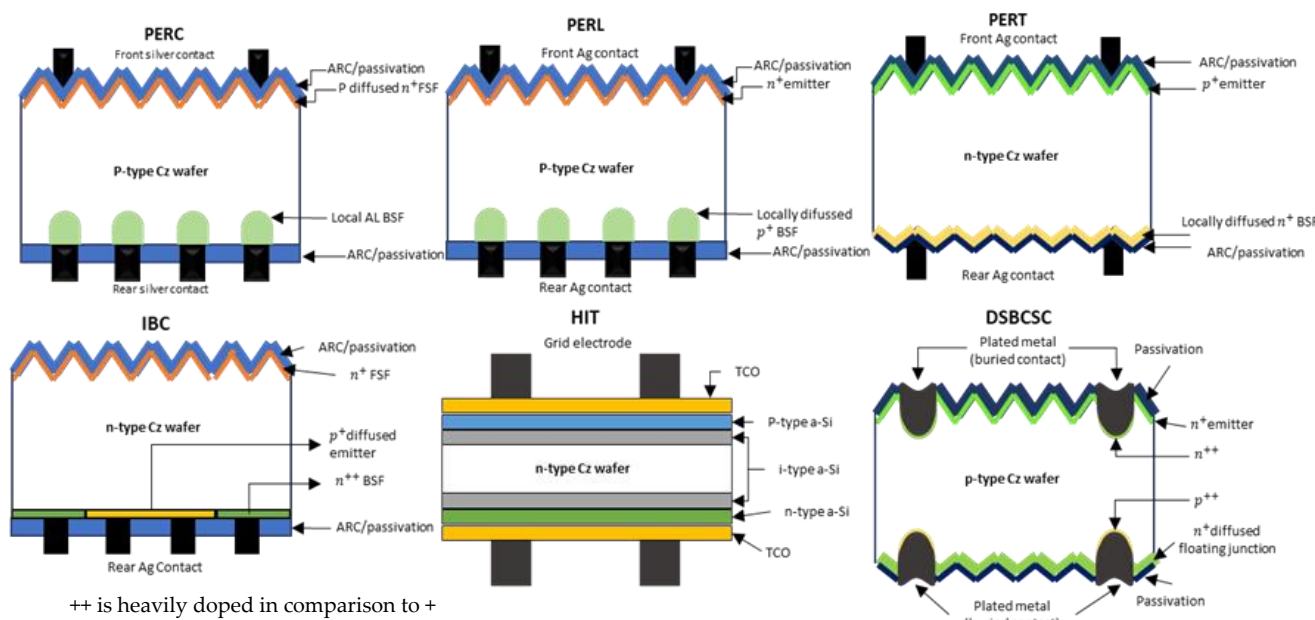


Figure 2. Structure and configuration of bifacial and monofacial photovoltaic cells (adapted from [24]).

The most common encapsulation in bPV is the glass/glass structure, which allows absorption from both sides [25]. However, bifacial cells with glass/backsheet encapsulation deliver more power and current compared to glass/glass in STC measurements, where mainly front illumination is adopted. The reasons for this are first, the transmittance of the bifacial cell for longer wavelengths and the result in a back-scattering within the backsheet and, secondly, backsheet scattering in the cell gap region bring reflection at the glass to air interface [26]. However, the glass/glass encapsulation provides more power in real outdoor conditions due to the rays reflected by the albedo on the rear side that cannot be converted into electricity in the glass/backsheet configuration.

Several technologies have also been developed to take full advantage of bifacial PV cell structures by minimizing optical and resistive losses. In principle, resistive losses can be decreased by using small busbar wires or a combination of busbars, which will eventually decrease the series resistance as a result of the presence of a longer current path plus shorter finger wires (or much thinner) [24–26]. Half-cell modules can also be one of the solutions to reduce resistive power loss [27]. Small wires and multi-busbars can also be a good option to reduce optical loss by reducing shading in the active area of the cell and minimizing the reflectance and absorbance of the beams in the inactive area. In addition, an infrared (IR) reflective coating on the rear glass of the bifacial glass/glass module would reduce the transmission loss. The white reflective coating on the rear glass can lower the transmission loss of the cell gap. By combining these two, a current gain of about 4% can be achieved [28].

The predicted high share of the bifacial technology in the market has prompted several companies and research groups to develop improved bifacial PV cells with different bifacialities and efficiencies. The most prominent PV cells on the market are a HIT heterojunction, an IBC interdigitated back contact, a DSBSC double-sided buried contact, a PERC passivated emitter back contact, a PERL passivated emitter back contact, and a passivated emitter back contact with full diffusion (PERT) [5]. Figure 3 shows the structures of the different cells with the available bifaciality and efficiency. The maximums were achieved by the heterojunction bPV cell, which will result in higher power output compared to the others.



Bifacial PV cell	PERC	PERL	PERT	IBC	HIT	DSBSC
Characteristics	<ul style="list-style-type: none"> Bifaciality: 80% Efficiency : 19.4 – 21.2% (Front), 16.7 – 18.1% (Rear) 	<ul style="list-style-type: none"> Bifaciality: ≥ 89% Efficiency : 19.8 (Front) 	<ul style="list-style-type: none"> Bifaciality: ≥ 85% Efficiency : 19.5 – 22% (Front), 17 – 19% (Rear) 	<ul style="list-style-type: none"> Bifaciality: 75% Efficiency : 23.2% 	<ul style="list-style-type: none"> Bifaciality: >95% Efficiency : 24.7% 	<ul style="list-style-type: none"> Bifaciality: 75% Efficiency : 22%

Figure 3. Non-exhaustive list of bifacial photovoltaic cell technologies adapted from [5].

2.2. Fundamental Solar Cell Losses

As with monofacial photovoltaic modules, bPV modules produce electricity by absorbing a portion of the sun's rays and dissipating the remainder through losses of energy inside the cell or from the cell to the module [29]. Losses incurred from the cell to the module are mainly due to the series resistance, reflected and/or transmitted light. These losses result in a decrease in the total output power of the module compared to the sum of the output power of the bPV cells [30,31]. Losses in the cell, based on the lifetime of the carrier, can be grouped as generation, transport, and recombination losses [32].

Carrier generation process losses: (i) optical losses corresponding to the fraction of incident solar radiation energy that is reflected by or transmitted through the cells [24], and (ii) spectrum mismatch losses due to the difference between the spectral responses of the PV reference solar cell and the outdoor test PV modules [25].

- Carrier transportation process losses consist mainly of: (i) series resistance losses, due to the loss in the transport of carriers in their paths due to collision with atoms or other carriers [26]; (ii) the shunt resistance loss can be associated with the recombination process, which conducts the generation of heat and is proportional to the loss of photocurrent; [27](iii) The Carnot loss is defined as the minimum energy required to separate photo-generated charges [26]; and (iv) the angular mismatch loss referred to the energy loss caused by the mismatch between the absorption and emission solid angles [24].
- Carrier recombination process losses: emission loss corresponds to the photons emitted by the cells resulting from radiative recombination and non-radiative recombination loss [24].

2.3. Bifacial Technology Performance Parameters

The most important parameters which characterize bifacial photovoltaic technology are:

- The power conversion efficiency (η_{Bifacial}) is the ratio of the generated electrical power P_m (W) to the incident light power E (W/m^2) under one sun with a ($G_{\text{ref}} = 1000 \text{ W/m}^2$) or more. It is measured separately for the front and rear faces. In general, it is calculated at the maximum power point, P_m , in W, using the area of the solar cell (A , in m^2). This definition can extend to define the bifacial module efficiency as the power produced divided by the total irradiance power received by the working surfaces of the module. The efficiency of the bPV cell can go from 19.4% for PERC to 24.7% for HIT at the front side, and from 16.7% for PERC to 19% for PERT at the rear side (Figure 2) [5].

$$\eta_{\text{Bifacial}} = \frac{P_{m,\text{front/rear}}}{E_{\text{front/rear}} * A} \quad (1)$$

- The bifaciality factor (φ) defines the ratio of the device's front and rear responses under the same conditions. This parameter essentially determines the additional power that can be generated by the rear irradiance. In the literature, there are different approaches to defining the bifaciality factor, based on power, current density, voltage, or efficiency. The most common one is the ratio between the power of the rear of the module and the front under STC conditions [8]. The main equations to define bifaciality are as follows:

$$\varphi_{J_{\text{sc}}} = J_{\text{sc,r}} / J_{\text{sc,f}} \quad (2)$$

$$\varphi_{V_{\text{oc}}} = V_{\text{oc,r}} / V_{\text{oc,f}} \quad (3)$$

$$\varphi_{P_{\text{max}}} = P_{m,r} / P_{m,f} \quad (4)$$

$$\varphi_{\eta} = \eta_r / \eta_f \quad (5)$$

where J_{sc} is the current density, V_{oc} the voltage, and P_m the power and η the efficiency. The subscripts "f" and "r" indicate the front and rear surfaces, respectively. The main

characteristics that determine the bifaciality factor of a bPV cell are the rear surface texture and antireflection coating (ARC) [28,29], the metal coverage of the rear side contact [30], the rear side back surface field (BSF) doping and passivation [31], and the base resistivity and lifetime of the solar cell [32]. The maximum bifaciality factor was achieved for Si heterojunction bPV cells with values ranging from 85 to 95%, followed by n-PERT from 75 to 90%, and then by the P-PERC from 65 to 80% [8].

- The bifacial gain (BG): an appropriate way to illustrate the importance of bifaciality is to analyze the bifacial gain, which is defined as the difference in energy yield when comparing bifacial and monofacial devices with identical installation configurations. Generally, this comparison is based on the energy yield, expressed in KWh/KWp [33].

$$BG(\%) = \frac{Y_{\text{bifacial}} - Y_{\text{monofacial}}}{Y_{\text{monofacial}}} \times 100 \quad (6)$$

$$BG_{\text{optical}} = G^{\text{Rear}} / G^{\text{Front}} \quad (7)$$

where Y_{bifacial} is the energy yield of a PV system with bifacial modules and $Y_{\text{monofacial}}$ the energy yield with monofacial modules in the same conditions (site, configuration, and time period). A similar factor is the bifacial optical gain in Equation (7), which is defined as the ratio of the rear (G^{Rear}) to the front (G^{Front}) irradiances [34]. The bifacial gain depends mainly on the ground albedo and the distance between rows. The smaller the distance between the module rows, the lower the BG, and a high albedo will result in a higher BG [34].

- The spectral response (SR): as the monofacial cells photovoltaic cells, bPV cells have a spectral response (SR in A/W) representing the fraction of the available irradiance that is converted to current [35]. The front and rear of the bPV cell may show a slight difference in spectral response (Figure 4) [36], mainly due to the difference between the two sides in passivation and metal contacts.
- The ground albedo (α): ratio of reflected radiation to the radiation from the sky dome. It is common to assume the albedo of the ground surface as a constant for monofacial PV systems, due to the limited contribution of reflected irradiation from the ground. In general, the contribution of reflected radiation on the ground is less than 3% for most monofacial PV systems and can be less than 1% for systems with a slope of less than 25° [33]. In fact, the albedo is spectral and angle-dependent, and because of the significant rear reflected irradiance importance for bPV systems, the spectral albedo is typically adopted (Figure 5). The constant percentage of reflected light α can be calculated as a function of spectral reflectivity $A_r(\lambda)$ as [37]:

$$\alpha = \frac{\int G(\lambda) A_r(\lambda) d\lambda}{\int G(\lambda) d\lambda} \quad (8)$$

where $G(\lambda)$ is the spectrum incident on the surface. The reflected light can be simply calculated by multiplying the constant albedo by the broadband incident spectrum at this point.

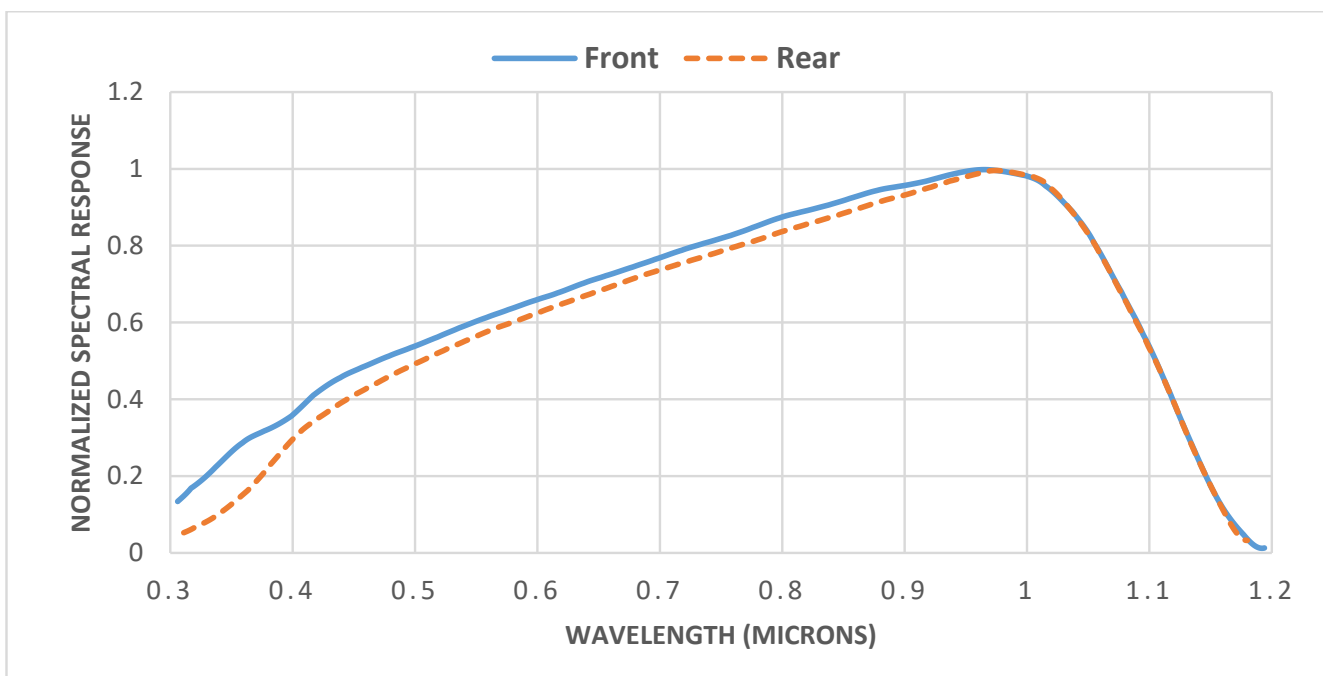


Figure 4. Normalized spectral responses of the front and rear of a mono-crystalline silicon bifacial module [36].

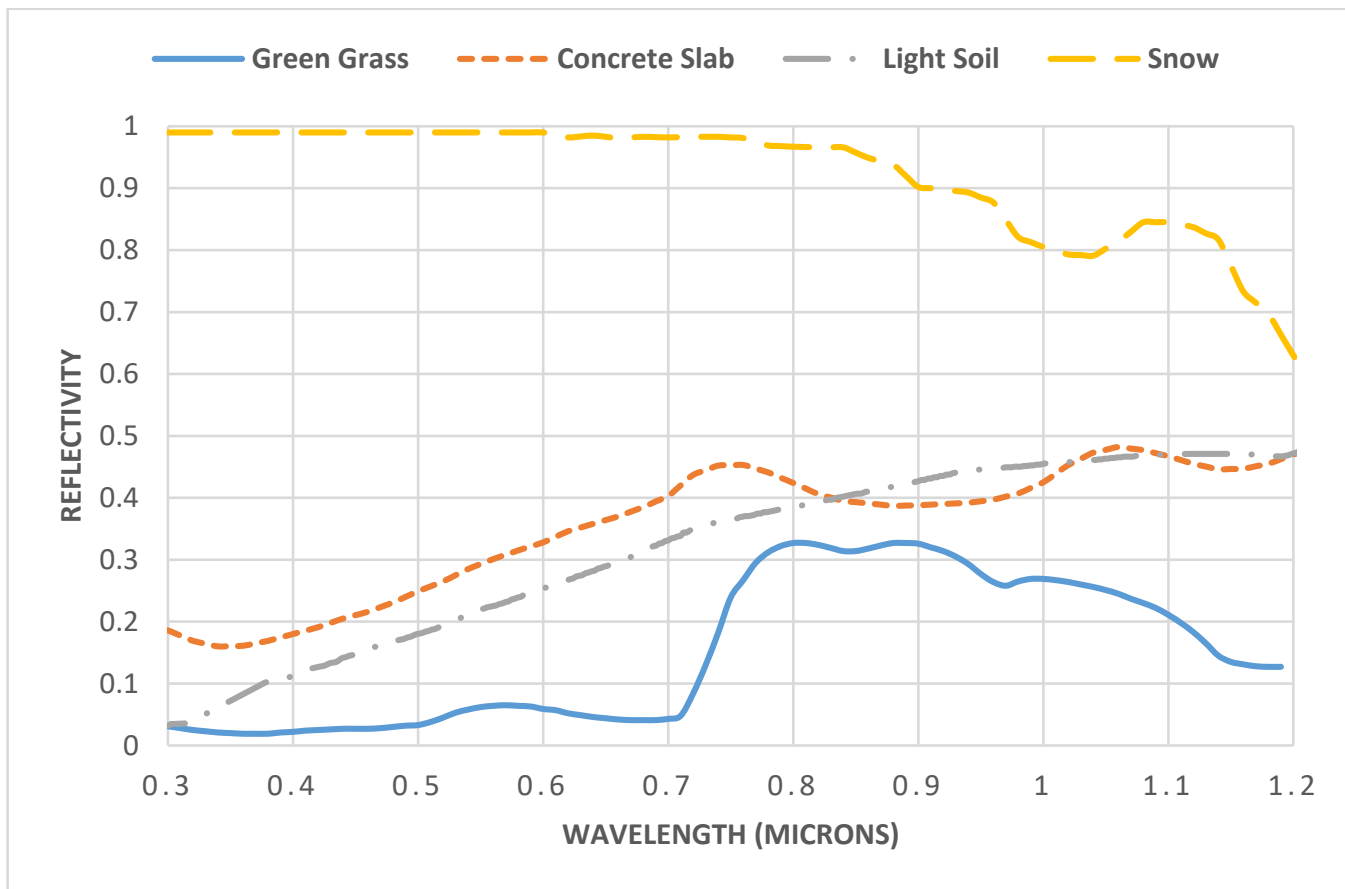


Figure 5. Spectral reflectance of four ground surfaces from SMARTS in the C-Si spectral range [38].

3. b-PV Modeling Methods

There are various models for predicting the performance of bifacial PV systems, which are reviewed in this section. The models are typically one of three types. Optical models calculate the irradiance received by a bifacial PV module from the front and rear. Thermal models calculate the cell or module temperature. Electrical models estimate the electrical output of a PV module.

3.1. Optical

3.1.1. Front-Side Irradiance

The front-side irradiance in bPV, (G^{Front}) is actually similar to the monofacial, and is composed of three components: direct, diffuse, and reflected irradiance. In some cases, such as for SMARTS, there is no need for further calculation because the front-tilted global irradiance can directly be obtained. However, if only horizontal irradiance is available, according to Khoo et al. [39], the front-side irradiance of bifacial PV modules may be simulated using the same optical model that is used to simulate monofacial photovoltaic systems. The total irradiance on the front side of an inclined (tilted) bifacial photovoltaic module can be expressed as follows:

$$G^{\text{Front}} = G_b R_b + G_{d,\text{tilt}} + \alpha \cdot GHI \left(\frac{1 - \cos(\beta)}{2} \right) \quad (9)$$

where G_b is the beam irradiance on a horizontal surface and R_b is the ratio of the beam irradiance on the tilted surface to that on a horizontal surface at any given time. $G_{d,\text{tilt}}$ is the total tilted diffuse irradiance and, in the literature, there are numerous formulas available [40,41]. The Perez et al. [42] model is the recommended model since it takes into account the three diffuse irradiance elements (isotropic sky diffuse, circumsolar diffuse, and horizontal brightness). Thus, the total inclined diffuse irradiance is given by the Perez et al. model as follows:

$$G_{d,\text{tilt}} = G_d \left(\frac{1 + \cos(\beta)}{2} \right) (1 - F_1) + F_1 R_b + F_2 \sin \beta \quad (10)$$

where G_d is the diffuse horizontal irradiance, β is the module tilt angle, F_1 is the circumsolar brightness coefficient, and F_2 represents the horizon brightness coefficient. Both F_1 and F_2 are linked to the sky irradiance conditions, which are described by three variables: the zenith angle of the sun θ_z , the sky brightness index ϵ , and the brightness index Δ . The last term is the diffuse component that is driven by reflection from the ground. It is generated from an isotropic model proposed by Ineichen et al. [42,43]. α is the albedo (or ground reflectance), which is usually assumed to be uniform over the entire ground surface underlying the module [44]. $[(1 - \cos\beta)/2]$ is the view factor from the front of the bifacial PV module to the ground, under the assumptions of (1) infinitely long rows; (2) absence of shadows on the ground; (3) the ground is horizontal; and (4) the ground is a Lambertian reflector (independent of direction) [45]. Irradiance data used in the model can be obtained from databases such as SolarGIS [46], Meteonorm [47], and PVGIS [48] or from tools, such as SMARTS software [38], or they can be measured on-site.

3.1.2. Rear-Side Irradiance

Modeling the rear irradiance is more complicated because it is a combination of diffuse and direct irradiance reflected from the shaded and unshaded ground. The most used methods in the literature to simulate it are the view factor and ray tracing methods.

The View Factor Model

The view factor was first brought to measure the portion of the radiative heat flux leaving surface A and reaching surface B [49]. It is a purely geometrical parameter and has also been applied in the calculation of the irradiance reflected by one surface and perceived

by the other. Photovoltaic panels are generally used in rows in the solar field, which means a negligible module width compared to the row length, which allows for considering a row of modules of infinite length. Then, the Hottel cross-string rule can be adopted [50]. This rule allows us to calculate the view factor from surface A to surface B (Figure 6) as:

$$F_{A \rightarrow B} = \frac{\sum \text{Crossed strings} - \sum \text{Uncrossed strings}}{2 \cdot \text{Source string}} = \frac{CF + DE - CE - DF}{2 \cdot CD} \quad (11)$$

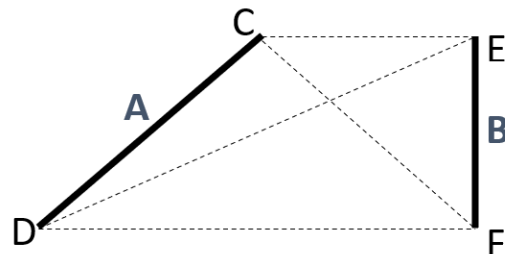


Figure 6. Calculation of view factor: two surfaces of infinite length applying Hottel's crossed-string rule.

To calculate the rear irradiance of a row of bifacial modules of length L mounted with a tilt angle β and with a module-to-ground clearance h (Figure 7), three view factors ($F_{\text{Sky}}^{\text{Rear}}$, $F_{\text{unshaded ground}}^{\text{Rear}}$, and $F_{\text{shaded ground}}^{\text{Rear}}$) have to be determined. The rear irradiance can be obtained from Equation (12), which denotes the three components of the global tilted rear irradiance: beam, diffusion, and reflection:

$$\begin{aligned} G^{\text{Rear}} &= G_{\text{beam}}^{\text{Rear}} + G_{\text{diffuse}}^{\text{Rear}} + G_{\text{reflected}}^{\text{Rear}} \\ &= (GHI - G_d) \cdot R_{\text{beam}}^{\text{Rear}} + G_d \cdot F_{\text{Sky}}^{\text{Rear}} + GHI \cdot \alpha \cdot F_{\text{unshaded ground}}^{\text{Rear}} + G_d \cdot \alpha \cdot F_{\text{shaded ground}}^{\text{Rear}} \end{aligned} \quad (12)$$

where GHI , G_d represent the global and diffuse horizontal irradiance, $R_{\text{beam}}^{\text{Rear}}$ is the proportion of the inclined rear irradiance over the horizontal irradiance, and α is the albedo (or ground reflectance). A more detailed calculation of every term can be obtained from [49].

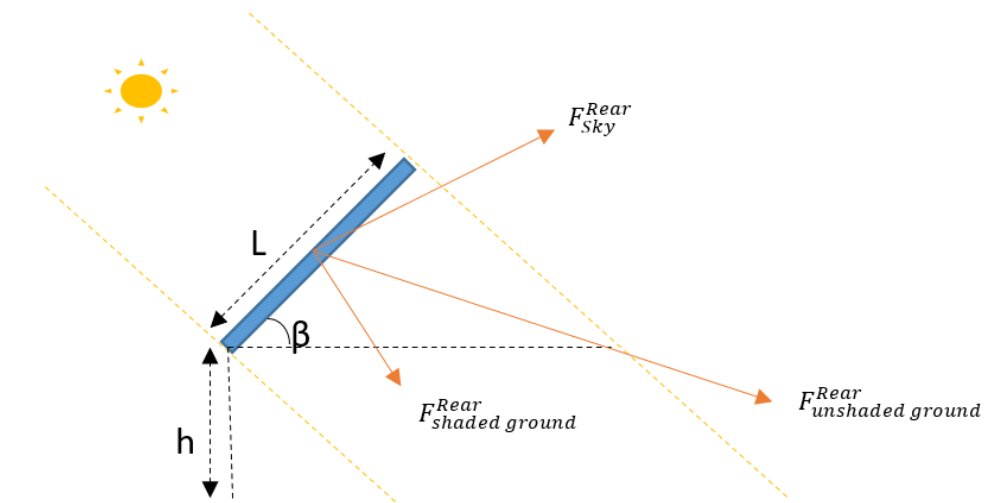


Figure 7. Schematic diagram of the rear-view factors of a bPV module.

Ray Tracing Model

Ray tracing models track light from the source to the intercepting surface (forward ray tracing) or from the surface of interest to the source (inverse ray tracing). Models are often based on a Monte Carlo approach which simulates thousands of rays and then uses optical physics to predict the way these rays interact on each surface of the model [50].

To predict the irradiance on the rear face of a bifacial photovoltaic panel, the ray tracing model needs inputs such as the geometry of the structure, the properties of the materials, and the position of the sun. There are different tools that perform simulation based on the ray tracing method. These include free software packages, such as Radiance (inverse ray tracing application) [51] and commercial ones, such as Trace PRO [52] and COMSOL (forward ray tracing application) [53]. The primary benefits and drawbacks of the two bifacial simulation approaches are displayed in Table 1 [54].

Table 1. The main advantages and disadvantages of bifacial simulation approaches.

	Advantages	Disadvantages
View Factors	<ul style="list-style-type: none"> The view factor concept can be easily and quickly implemented on regular mounting geometries. The inhomogeneity of the bifacial module's rear irradiance can be replicated using the view factor approach. The computing time is very low even for a full-year simulation with a time step of one hour. 	<ul style="list-style-type: none"> The accuracy is affected by the meshing on the module's rear side. Difficulty in taking into account irregular geometries of mounting structures and uneven ground surfaces. In the case of large bifacial PV systems, the simulation time can be excessively long.
Ray-Tracing	<ul style="list-style-type: none"> Ray tracing is more convenient for modeling the inhomogeneity of bifacial module irradiance. The impact on the rear irradiance of structures and the module frames can fully be taken into account. 	<ul style="list-style-type: none"> In comparison to the view factor approach, the implementation of ray tracing in a modeling tool is more challenging. Ray tracing simulations have a relatively high computational power need, which causes them to take a long time to run. Accurate knowledge of soil properties is necessary to correctly calculate spectrally and angularly reflected radiation, which is not always available.

A comparison of the accuracy between the ray tracing (Radiance), the view factor method, and the measurements has been made in [55] for two consecutive days at solar noon and for different clearances for different sensor positions from the lower to the upper part of the module, respectively, A, B, C, and D. The authors found that the view factor model agrees better with measured values for a clearance of 0.6 and 0.15 m than the RADIANCE software. From the data in [55], in (Figure 8) the errors were calculated and show that in general the view factor grants lower errors. However, ray tracing is able to obtain more details than the view factor model, as it takes into account the cell-to-cell gaps and/or the shading produced by the junction box at the back of the module. In spite of this, ray tracing can be of great interest for novel applications, such as agrivoltaic or building integration, since the reflected surface can show a high inhomogeneity (trees, walls, etc.). For example, agrivoltaic (APV) deals with complex geometries (crops or trees) that cannot be simulated with VF assuming that the vegetation is uniformly distributed. The same occurs in greenhouses, and RT can help to overcome this problem.

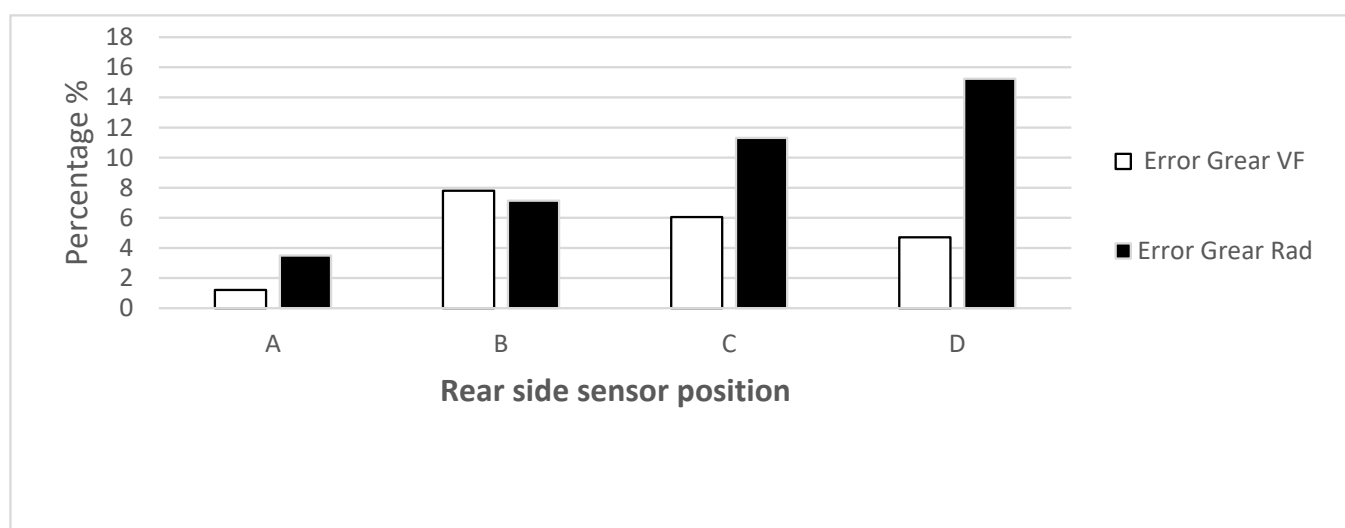


Figure 8. Rear irradiance distribution error for the ray tracing and view factor methods for four positions of measurement (A, B, C, and D).

There is another approach to bifacial modeling based on the prediction of energy performance by empirical modeling. This uses different experimental results to develop the coefficients of the best-fit model as in Equation (13) [54,56].

$$BG = A \times (\beta) + B \times (h) + C \times (\alpha) \quad (13)$$

where A (/deg) is the fit coefficient for the tilt angle β , B (/meter) is the fit coefficient for the ground to module clearance h , and C (/%) is the fit coefficient for albedo α . For a particular set of applications, there is good agreement between the results of the experiments and the models. For example, Jose E [56] developed a model which shows an annual energy difference of a maximum of 7.2% and a minimum of 0.52% for different conditions of slope, altitude, and albedo. Even with this accuracy, there have been very few attempts to forecast the performance of bifacial plants through empirical models. The reason is the shortage of experimental data to build accurate and reliable empirical models. Another reason for the limited application of the empirical method is that it can only estimate the bifacial gain for a given period of time and not the power values of the bifacial modulus for a given period of time, such as the Raytracing and view factor methods. However, this method can be of great interest to account for the bifacial contribution at the system or plant level due to its simplicity. From an engineering point of view, this method is preferable due to its easy applicability.

3.2. Electrical

The electrical performance of bifacial PV technology is the result of the combination of the front and rear characteristics under the same conditions. In the literature, there are three methods for the electrical modeling of bPV technology: the single point power models, which are the most basic; additionally, the equivalent circuit model and the characteristic point model, which are all used to predict the I-V curve as in (Figure 9) [57].

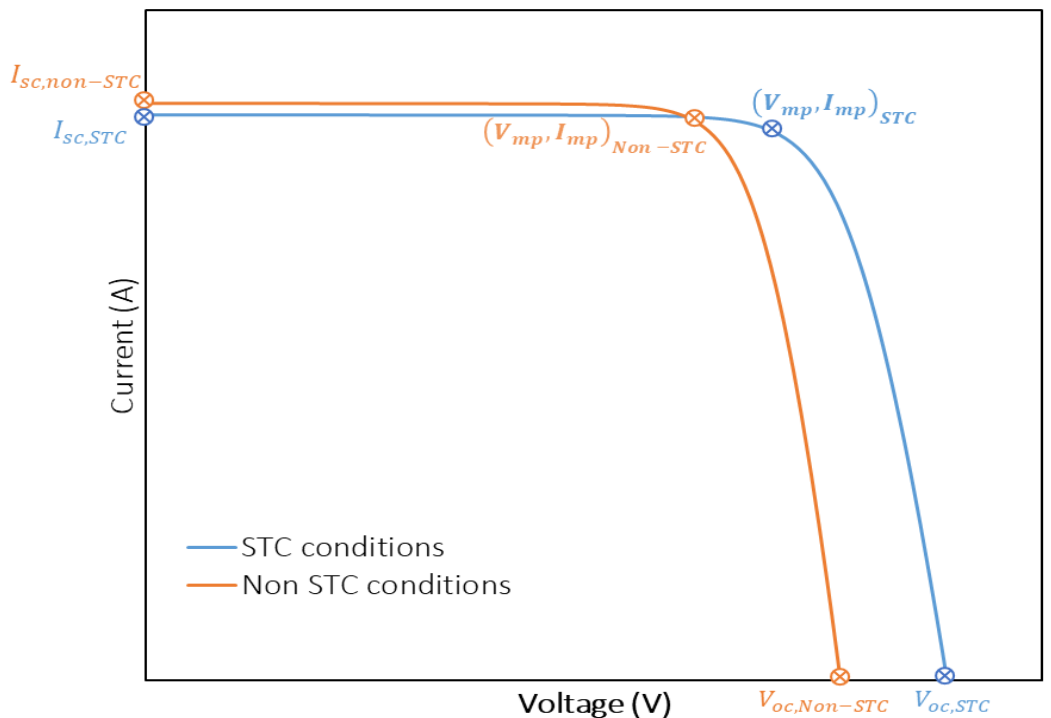


Figure 9. The characteristics and parameters of a typical I-V curve.

3.2.1. Single Point Power Model

This model simulates the total power output of the bifacial solar modules as [57]:

$$P_{PV} = G^{\text{Front}} * A * \eta^F + G^{\text{Rear}} * A * \eta^R \quad (14)$$

where P_{PV} is the total output power of the bifacial solar module. G^{Front} and G^{Rear} can be calculated using the optical model as in the previous section. Otherwise, it can be measured with two pyranometers, one for each side, or with an albedometer. η^F and η^R are the electrical efficiencies of the front and rear faces of the bifacial photovoltaic module and A is the module area. This model is general and can be used for any PV technology. For the front and rear electrical efficiencies, $\eta^{F,R}$ can be calculated as a function of the efficiency $\eta_{\text{stc}}^{F,R}$ at standard conditions and the cell temperature T_{Cell} [57] as Equation (15):

$$\eta_T^{F,R} = \eta_{\text{stc}}^{F,R} * (1 + \beta_T * (T - T_{\text{stc}})) \quad (15)$$

where β_T is the temperature coefficient of the bPV module and STC stands for standard test conditions (STC, solar irradiance $G_{\text{ref}} = 1000 \text{ W/m}^2$, cell temperature $T_c = 25^\circ\text{C}$, and air mass AM = 1.5).

3.2.2. Characteristic Point Model

In this model [57], the short-circuit current (I_{sc}) and open-circuit voltage (V_{oc}) for the front and rear sides of the bifacial PV module can be separately determined for the specified operating conditions. The dependence of I_{sc} on incident irradiance is linear, whereas logarithmic for V_{oc} . The short-circuit current of the bifacial module (I_{sc}) and its open-circuit voltage (V_{oc}) are thus given by:

$$I_{sc} = I_{sc}^F + I_{sc}^R \quad (16)$$

$$V_{oc} = V_{oc}^F + \left(V_{oc}^R - V_{oc}^F \ln \left(\frac{(I_{sc}^F + I_{sc}^R)}{I_{sc}^F} \right) \right) / \ln \left(\frac{I_{sc}^R}{I_{sc}^F} \right) \quad (17)$$

$$P_{mpp} = FF * V_{oc} * I_{sc} (1 + \beta_T (T - T_{stc})) \quad (18)$$

where P_{mpp} is the power output at the maximum power point (MPP), whereas FF is the fill factor.

3.2.3. Equivalent Circuit Model

This model is more accurate than those mentioned above [57] and is the most widely used in academic circles. In the literature, there are several equivalent circuit models that differ in the number of diodes and parameters. These have been summarized by Tossa et al. [58]. These models calculate the mean parameters of the I–V curve of bPV under STC conditions. The most broadly used model approach in the literature is the single diode model (SDM) (Figure 10), which includes a series resistance (R_s), a shunt resistance (R_p), and linear independent current source in parallel to one diode [59]. In SEM, the following equation can be used for non-STC conditions:

$$I_{ph} = \frac{G}{G_{stc}} \left(I_{ph,stc} + \beta (T_c - T_{stc}) \right) \quad (19)$$

$$I_0 = I_{0,stc} \left(\frac{T_c}{T_{stc}} \right)^3 * e^{\left(\frac{qE_g}{T_{stc}} \left(\frac{1}{T_{stc}} - \frac{1}{T_c} \right) \right)} \quad (20)$$

$$R_s = R_{s,stc} \quad (21)$$

$$R_p = \frac{G_{stc}}{G} R_{p,stc} \quad (22)$$

$$V_t = \frac{T_c}{T_{stc}} V_{t,stc} \quad (23)$$

$$G_e = G^{\text{Front}} + \varphi G^{\text{Rear}} \quad (24)$$

where E_g is the band gap, q is the electric charge and G_e is the bifacial equivalent irradiance defined as the irradiance received by the bifacial module and contributing to current generation.

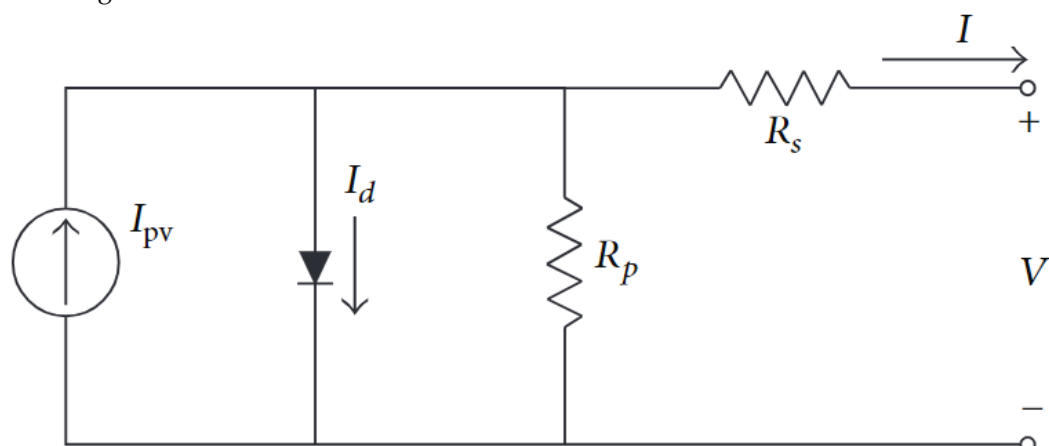


Figure 10. Circuit diagram of the SDM.

3.3. Thermal

Unlike irradiance, which can be measured with a pyranometer, the PV cell temperature cannot be measured directly with a thermocouple. Therefore, the thermal behavior of bPV modules has to be modeled. There are different models in the literature to simulate the bPV cell temperature. The most frequently used models are discussed in this section.

3.3.1. NOCT Model

This model was first used for monofacial technology [60] taking into account only frontal irradiance, and then extended for bPV cells [61]. However, large differences were

observed experimentally. On the other hand, using total irradiance (front + rear) led to more accurate results [61]. This model only takes into account the variation of bPV cell temperature with total irradiance and negates the effect of wind speed by means of the following expression:

$$T_c = T_a + \frac{T_{NOCT} - 20}{800} \times (G^{\text{Front}} + G^{\text{Rear}}) \quad (25)$$

T_{NOCT} is the nominal operating temperature of the cell in °C, specified by the manufacturer and T_a is the ambient temperature. In [62], a wind speed correction of this model is available.

3.3.2. Sandia Model

This model has proven to be very adaptable and fully suitable for engineering and system design purposes, as it provides the expected operating temperature of the module with an accuracy of approximately ±5 °C [63]:

$$T_c = T_m + \frac{G^{\text{Front}} + G^{\text{Rear}}}{G_{\text{ref}}} \times \Delta T \quad (26)$$

$$T_m = (G^{\text{Front}} + G^{\text{Rear}}) \cdot (e^{k1+k2 \cdot U_w}) \quad (27)$$

where G_{ref} is the irradiance under STC conditions (1000 W/m²), ΔT is a temperature difference parameter, defined as the difference in temperature entering the module and the cell, U_w represents the wind speed at a standard height of 10 m, and T_m is the module temperature bPV. $k1$ and $k2$ are parameters that depend on module structure, materials, and module mounting configuration. A list of representative values of these parameters for various types of modules and common configurations can be found in [64].

3.3.3. PVsyst Model

This thermal model is used in the commercial software PVsyst and is derived from the Faiman model Equation (28) [65]:

$$T_c = T_a + \frac{\alpha_a \cdot G_T \cdot (1 - \eta)}{U_0 + U_1 \cdot U_w} \quad (28)$$

where α_a is the absorptivity, η is the electrical efficiency of the bifacial photovoltaic module, U_0 is the coefficient of heat transfer (W/m²K), and U_1 is the component of convective heat transfer (W/m³sK). The difference between this model in the monofacial version is the temperature changes with the total irradiance G_T , which in this case the sum of G^{Front} and G^{Rear} .

3.3.4. Equivalent Thermal Circuit Model

This model is based on thermal resistances. Three categories of resistance are used: radiative, convective, and conductive. This model can simulate the temperature of different cell layers such as the top and bottom (EVA) beside the bPV cell temperature [66]. Based on the equivalent thermal circuit illustrated in (Figure 11) [66], the cell temperature can be determined through the following expression:

$$C_{p,PV} \delta_{PV} A \rho_{PV} \frac{dT_C}{dt} = (\tau_g \cdot G_T \cdot A - P_{PV}) - \frac{T_C - T_{EVA1}}{R_{PV-EVA1}} - \frac{T_C - T_{EVA2}}{R_{PV-EVA2}} \quad (29)$$

where $C_{p,PV}$, δ_{PV} and ρ_{PV} are the specific heat (J/(kg K)), thickness (m), and density (kg/m³) of the PV layer, respectively. τ_g is the glass transitivity (%), T_{EVA2} is the lower EVA temperature (K), and $R_{PV-EVA2}$ is the conductive thermal resistance between the PV layer and lower EVA (K/W).

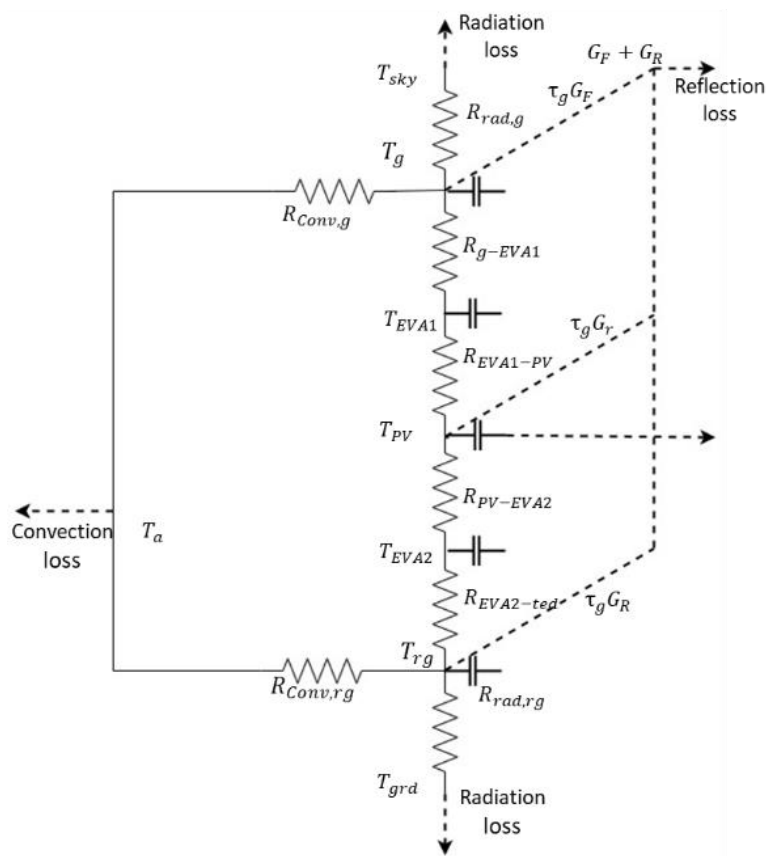


Figure 11. Equivalent thermal circuit of the bPV module adapted from [66].

3.3.5. Regression Model

This model is based on a multilayer mathematical model suitable for estimating the temperature of the bifacial PV cells with the following relationship [67]:

$$T_C = -22.1499 + 0.0300G_T + 1.9839T_a - 0.0142U_w \quad (30)$$

This equation considers the contribution of solar radiation incident on the rear side of the bifacial PV module. The output of this model is the average temperature of the bPV cell as a function of solar radiation G_T (W/m^2).

4. Bifacial Technology Applications

4.1. Agrivoltaic

The definition of agrivoltaics is the simultaneous use of land for the production of electricity through photovoltaic modules and agricultural production. This combination offers a number of symbiotic benefits, such as the reduction of water balance and better resistance to climatic effects, such as excess heat and drought [68,69]. Some innovative technologies have been used for APV, such as concentrator photovoltaic (CPV) modules [70], which use direct solar rays and diffuse solar rays separately for efficient dual use of the land. Direct irradiance is used for electricity production through the CPV panels and diffuse irradiance is used for crop photosynthesis under the photovoltaic panels. The main drawback of this technology is mass production, which results in high costs [71]. Semitransparent photovoltaics were also used for APV, either with spectral semitransparency with selective use of wavelengths [72], or with regional semitransparency by splitting the portion of the received solar rays between the PV panel and the crop below [73]. The main limitation of this technology is that it is still premature for large-scale installations due to its low efficiency [74], and significant degradation constraints [75]. The application of bifacial technology in the APV offers advantages in different aspects, as it can produce electricity by simultaneously

receiving direct sunlight and rear-reflected light from the ground or plants. The efficiency of the bifacial APV can reach up to 24% [76]. The current LCOE of bifacial photovoltaics is also lower than that of conventional monofacial photovoltaic systems [77]. All this makes the bifacial APV a potential solution for combining photovoltaics and agriculture. This section covers the definition of the main parameters defining the performance of APV systems, with an existing bifacial agricultural systems (Table 2).

4.1.1. APV Main Parameters

Photosynthesis is the natural process used by plants to capture energy from the sun and convert it into organic matter, which is then used to sustain almost all life on Earth [78]. Plant growth is dependent mainly on photosynthesis. The accumulation of organic matter by the process of plant photosynthesis is called the net photosynthetic rate (P_n), and is often used to evaluate the state of plant growth and photosynthetic capacity. The main factors affecting the rate of photosynthesis are light intensity, carbon dioxide concentration, soil and ambient temperature and humidity [79]. Similarly, to photovoltaic cells, the absorbance of the plant leaf depends on the spectral distribution of the incident light. The part of the light spectrum used by the plant for photosynthesis is called photosynthetically active radiation (PAR) ($\mu\text{mol}/\text{m}^2 \text{ s}$) [80], and is defined as between 400–700 nm wavelengths. For the processes of respiration and photosynthesis, a minimum light intensity is required, which is called the light compensation point (LCP), and, conversely, above a certain level of light intensity it is called the light saturation point (LSP) (Figure 12). Additional light does not enhance photosynthesis and the extra energy is converted to heat, which can reduce productivity [81].

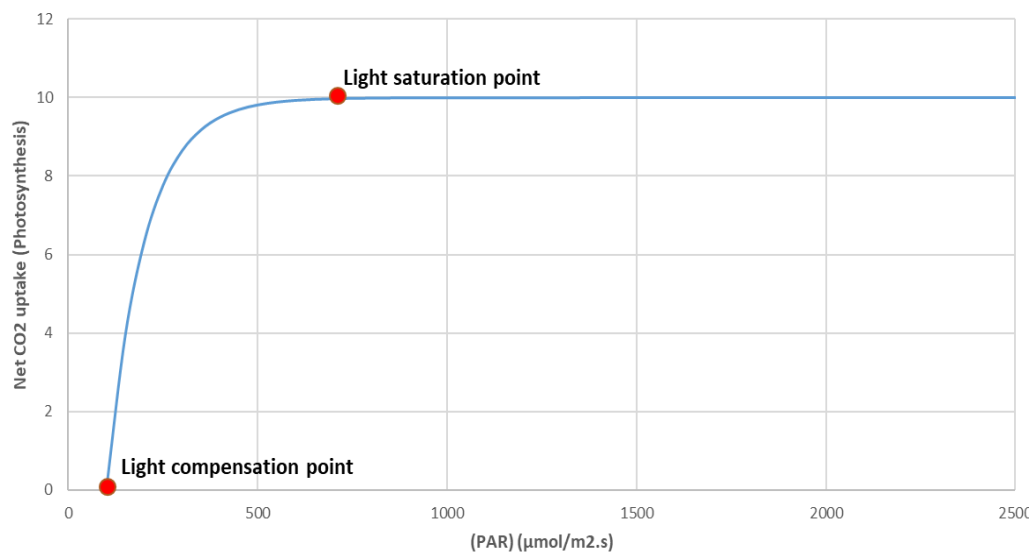


Figure 12. Photosynthesis light curve response showing the LCP and LSP points.

In addition to environmental conditions, genetic factors, such as the carbon assimilation pathway, greatly influence the photosynthesis process. Based on plant genetics, plants can be divided into C3, C4, and CAM species [82]. In agrivoltaics, the partitioning of the amount of incident light between the PV panel and the plant can decrease the light intercepted for the photosynthesis process, thus requiring species that are adaptable to low incident light. C3 species tend to saturate at low PAR [83]; they are also shade-tolerant and outperform C4 species in low-light conditions, making them the best choice for use under the PV plant [84].

The use of the installation of solar panels several meters above the ground surface has shown various advantages; for example, the temperature of the soil has decreased significantly [85], which favors the cultivation of plants. Similarly, the shading created by the photovoltaic panels slows down water evaporation, especially during the warm season,

leading to water savings of up to 14–29% depending on the shading level [86]. Another beneficial aspect of this agrivoltaic practice is the possible increase in the efficiency of energy production by reducing the temperature of the PV panels by 1 to 2 °C compared to the ambient temperature [87]. In addition, with APV, soil moisture remains approximately 5–15% higher in the agricultural system [88], depending on the frequency of irrigation, and the water used to clean the PV panels can be reused to irrigate agriculture [89]. All of this translates into an increase in water efficiency compared to the agricultural-only configuration. The APV can be more profitable compared to electricity or agriculture alone [90]. The co-location of photovoltaic and agricultural farms potentially can increase total site revenue by 2.5% to 24% over electricity income, depending on the location and farming type [91].

The land equivalence ratio (LER) is used to evaluate the performance of an agrivoltaic system (Equation (31)) [92]. The LER evaluates the energy and food ratios for the APV compared to standard photovoltaic agriculture and open field agriculture, respectively [93], as:

$$\text{LER} = \frac{Y_{\text{cropping-APV}}}{Y_{\text{monocropping}}} + \frac{Y_{\text{electricity-APV}}}{Y_{\text{electricity-PV}}} \quad (31)$$

where Y is the yield, monocropping system refers to single crop harvesting, PV refers to a standard photovoltaic plant, and APV stands for mixed agrivoltaic systems. An $\text{LER} > 1$ means that the APV system is more efficient than separating crops and PV for the same area. For example, an LER of 1.3 means that, by adopting an APV system, the production of electricity and food crops of a 100-ha farm will be equivalent to that of a 130-ha farm with separate productions. Another factor has been defined to assess the efficiency of irradiation spreading for a crop type and PV system called the light productivity factor (LPF) [94]. This factor is primarily used in design optimization to identify the optimal PV array density, panel orientation, and tracking configuration for a crop-specific PAR, which can predict the overall energy-food efficiency of the APV at the design stage.

4.1.2. Bifacial APV Configurations

Similar to any photovoltaic plant, the agrivoltaic farm consists of bifacial solar modules of height (L), mounted at a distance from the ground (h), and spaced by the pitch from row to row (P) (Figure 13). To achieve acceptable agricultural performance, PV array densities must be lower than those of conventional ground-mounted PV plants [95]. The radiation that is available at ground level increases together with the distance between rows. The ideal row spacing does not have a set value for all cases; instead, it varies from 3 m to around 10 m depending on the crop and the availability of sufficient land [96]. The usual configuration of an agrivoltaic system involves photovoltaic modules installed at a height of 2 to 5 m above the ground with a suspended structure [97]. The module's height depends on the specific agricultural activities underneath. The tilt and orientation of the modules in APV, similar to any photovoltaic plant, have different configurations (fixed tilt, single-axis tracking, and double-axis tracking), as discussed in the sub-sections below.

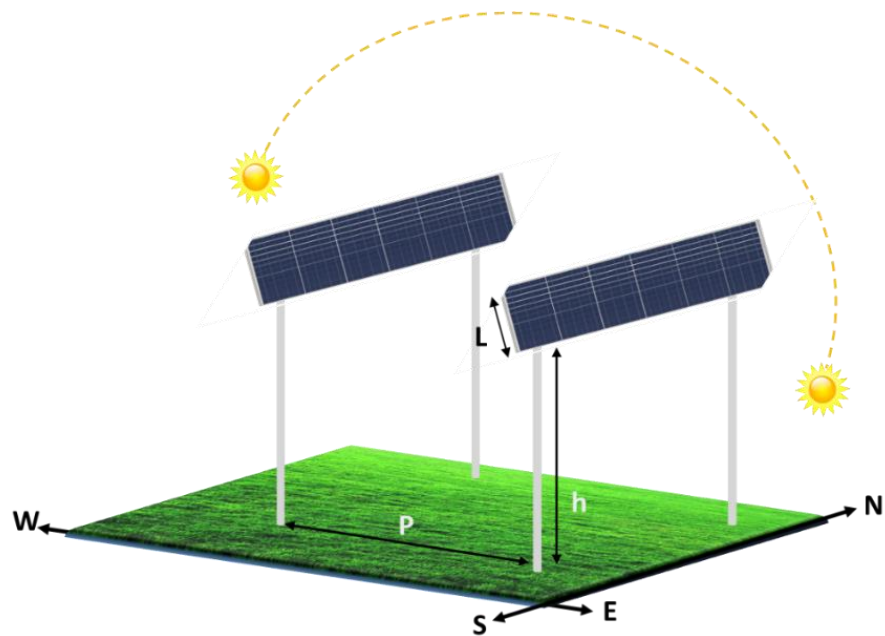


Figure 13. Schematic diagram of a bifacial fixed-tilt agrivoltaic farm.

Single Axis Tracking Configuration

The commonly used tracking configuration in APV systems is single-axis tracking. The one-axis scheme can be solar tracking (ST) when the module is aligned normally to the sun's rays or reverse tracking (RT) when the module's face is parallel to the sun's rays for moderate and shade-sensitive crops [98]. The tilt angle of the module with the tracking system is calculated based on the angle of incidence (θ_{AOI}) between the solar rays and the normal of the module. The target angle (θ_{AOI}) for ST is 0° , while for RT is 90° . It should be noted that two degrees of freedom are needed to maintain the module at normal incidence. However, single trackers have only one, and therefore act to minimize the angle of incidence rather than to maintain it at 0° [99].

A customized tracking (CT) scheme can also be adopted, which consists of switching between ST around noon and RT near sunrise and sunset, and RT for the other hours of the day [96]. Imran Hassan [100], in a study of APV farm performance of different orientations and tracking schemes in Lahore, Pakistan (31.5204° N, 74.3587° E), shows that ST maximizes energy production while ST minimizes it. The electrical energy produced by the bifacial modules (I_{PV}) in CT depends on the number of hours of adoption of the ST per day. The authors add that it ranges between the I_{PV} produced by the ST and the RT. Additionally, the global ground irradiance (G_{GR}) is maximum for the RT and minimum for the ST. A comparison of the same tracking scheme ST applied to systems of various orientations showed that the E/W modules produce more I_{PV} than the N/S [101]. Another study was conducted by Riaz Muhammad [102] in Lahore, for different tracking schemes and three different crops (lettuce, turnip, and corn). The results show a small difference in PAR between ST and RT in the morning and afternoon, but it becomes larger around solar noon. Even though the PAR that reaches the ground decreases by switching from RT to ST around noon, still values around the photosynthesis saturation active radiation PAR_{th} can be reached, while the CT scheme allows great flexibility to maximize PAR in a given month by switching between RT and ST. However, the adoption of half density of bifacial PV modules can make the difference between the PAR of different tracking systems negligible. As well, the ST limits yield for a precise PAR (Y_{PAR}) below 60% for full density, and using RT, Y_{PAR} recovers to >80%. For the half-density arrays, ST gives $Y_{PAR} > 80\%$ for all the three crops across all months. Furthermore, the adoption of CT can improve Y_{PAR} and this can be true even for full density arrays. Finally, the adoption of a scheme of tracking is an operation that can be carried out depending with other factors on the value

of photosynthesis active radiation PAR of saturation for the crops, and the shade tolerance of the crops.

Fixed Tilt Configuration

In the case of monofacial fixed-tilt north/south solar panels in the northern hemisphere, the PV system tilt angle is selected to optimize the annual energy yield, resulting in a value close to the latitude of the location [103]. For bifacial modules, the optimization of β may be different from that of monofacial PV panels, taking into account the β dependence of the height, albedo, system size, and time of the year [104]. The optimal tilt angle of the APV should be adjusted based on the desired balance for the distribution of sunlight between the PV panels and the crops. In [105], changing the tilt angle of an APV farm from 20° to 60° shows an increase in annual PAR of 13% and annual energy yield of 16%. This illustrates that adjusting the tilt angle can be a useful trade-off between crop and PV performance.

The Pitch Distance

The pitch distance in a solar PV system refers to the distance between rows in the APV installation. To study the effect of the pitch p (distance between rows), a parameter is been used called global ground radiation G_{GR} , defined at a specific crop height obtained as the percentage ratio between the light received under the cover of the panels and the total incident light without panels installed [104]. The energy produced by the PV modules increases with decreasing module density, i.e., with low pitch, and this is due to the high number of modules per pitch. However, the global ground radiation G_{GR} for crops decreases with increasing module density due to the high shading effect caused by the dense surface coverage of the PV modules [105]. A comparison of energy production of bifacial PV N/S and E/W was performed also in [103] at an inclination of 20°. The module density (p/h) was varied from 1 to 3. The monthly results showed that at low module density PV E/W had similar energy performance to PV N/S. As the panel density increased, PV N/S showed relatively higher energy output, and PV E/W provided a relatively higher G_{GR} and reduced the energy output for all panel densities. This gives an idea of the effect of the pitch on the agriculture and photovoltaic yields, which are complementary, and depends on the desired production.

The Elevation

The elevation of the photovoltaic modules h , intended as their vertical distance of the ground, is a major factor defining the heterogeneity of light at the crop level. The higher the modules are, the more homogeneous the daily irradiation on the ground is [69]. A high-height crop, such as corn, which can reach 2 m, allow homogeneity of irradiance to increase during the growing season, as the distance from the crop to the modules will be smaller. The elevation level can also affect the microclimate below the PV modules. For example, a variation of E from 0.5 to 2.7 m [106] causes significant differences in the average temperature near the PV modules. The average relative humidity and wind speed were also found to be different for different elevations. However, the choice of elevation depends also on the height of the crop and the machine used for harvesting [98], and using a high elevation also reduces the cost of the operation [19].

Table 2. List of operational bifacial agricultural photovoltaic systems.

No	Location	Electricity Yield	Capacity	PV Tracking	Cultivated Crops	Technology	Further Information	Refs
1	Donaueschingen—Aaser, Germany	4850 MWh/year	4.1 MWp	No	Meadow used for hay and silage	N-Pert (100%)	It is the largest bifacial agrivoltaic system in Europe. Was put into operation in 2020 and supplies electricity to 1400 households.	[107]
2	Eppelborn—Saarland, Germany	2150 MWh/year	2 MWp	No	Meadow used for hay and silage	N-Pert (60%), Heterojunction (40%)	It is the first large-scale bifacial PV system in Europe. It was launched in 2018 and supplies electricity to 700 households.	[107]
3	Channay, France	265 MWh/year	237 KWp	No	Test site for different arable crops and cattle farming	n-Type PERT/Heterojunction Bifacial Frameless	It is one of the first vertical bifacial agricultural power plants in France. It was put into operation in 2021 and supplies electricity to 80 households.	[107]
4	Valpuiseaux, France	124 MWh/year	111 KWp	No	Test site for different arable crops and cattle farming	n-Type PERT/Heterojunction Bifacial Frameless	It was put into operation in 2021 to supply electricity to 40 households.	[107]
5	Mälardalen University, Västerås, Sweden	37 MWh/year	33 KWp	No	Test site for different arable crops	n-Type PERT Bifacial Frameless	It was the first bifacial agrivoltaic farm in Sweden. It was put into operation in 2021 and supplies electricity to 11 households.	[107]
6	Seongang, South Korea	1300 KWh/year	30 KWp	No	No information	N-Pert (100%)	This is South Korea's first agrivoltaic plant, which started operating in 2020.	[107]
7	Saarland, Germany	31 MWh/year	28 KWp	No	Pastureland	Bifacial n-type cells	This is a pilot plant used for the validation of Next2Sun's vertical assembly system; launched in 2015.	[107]
8	Guntramsdorf, Austria	23 MWh/year	22.5 KWp	No	Arable land for the cultivation of potatoes	N-Pert (100%)	Austria's first ground-mounted agricultural photovoltaic-photovoltaic plants. It started in 2019.	[107]
9	Heggelbach, Germany	245 MWh/year	194 KWp	No	Winter wheat, potatoes, celery, and clover grass	No information	This project supplies electricity to 62 households and the preliminary result of the project showed an increase in the LER by more than 60%.	[108]
10	Bierbeek, Belgium	No information	185 W	One-axis solar tracking and fix tilt set-ups	Orchard crops, and pear trees	C-Si cells with transparent backsheet	Started in 2021; designed to demonstrate the viability of agrivoltaics in Belgium	[109]

4.2. Floating (Aquavoltaic)

Floating photovoltaic (FPV) solar power is a conception in which a solar photovoltaic system is placed directly on a body of water (Figure 14), rather than on the ground or the roofs of buildings [110]. The FPV installation is generally composed of a floating platform to keep the photovoltaic panels above the water [111], and a mooring system to keep the panels in the same position and prevent them from rotating or drifting away [111]. Additionally, solar photovoltaic modules (mono or bifacial) are used; although for this application more resilient modules, such as polymer, are required in salty environments [111]. The cables and connectors to extract the electricity from the solar photovoltaic installation and transport it to the shore have also to be adapted to the floating conditions. This means that the cables have to be properly coated with waterproof material because they are generally passing through water to reach the land [112].

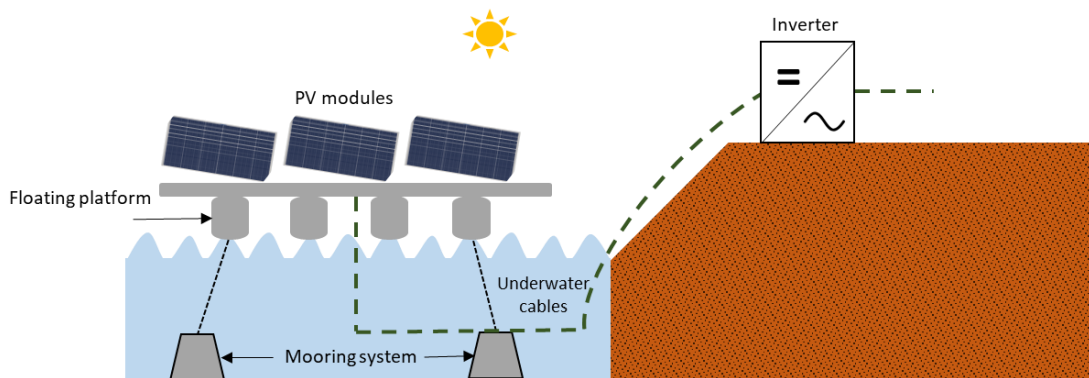


Figure 14. Schematic diagram of a floating photovoltaic power plant.

PV modules installed on water bodies can be very advantageous compared to PV systems installed on land. FPV can lead to savings in land costs, reduction of water evaporation, enhancement of water quality, minimizing the effect of dust, and lowering FPV temperatures due to the water cooling effect [113]. The bifacial floating photovoltaic system receives reflected irradiation from water. However, the albedo of water bodies is very low compared to the normal albedo of the soil [114]. Several studies suggest using a reflector under the bPV modules to overcome this drawback [115].

A comparison between monofacial and bifacial floating modeling and experimental data was performed in [116]. The installations had capacities of 3.84 KW for monofacial and 4.14 KW for bifacial modules. The results show that the bPV had a bifacial gain of 4.5% and 7.3% in Frankfurt (Germany) and Catania (Italy), respectively. Another comparison between mono and bPV floating PV systems was conducted in the tropical region of Lake Mahoni, Indonesia [116]. The total capacity of the installation was 9.36 KWp, divided into twenty-seven bPV panels and nine Mono PV panels. The bifacial strings showed better results with a maximum difference in electrical energy in May of 8.04% and a minimum in July of 6.13%.

Because of the young age of technology, there is limited field experience in FPV in general. The data regarding floating bPV are even fewer and, to the authors' knowledge, there are not many large commercial installations made in the world. However, this is expected to change, especially thanks to the falling prices of bPV modules. Currently, a 2.83 MW floating solar PV farm, with about 6900 bifacial modules has been installed in Ratchathani, Thailand [117]. The expected energy production is 4440 MWh.

4.3. bPV Vertical Application

Bifacial PV modules have different dual applications when used vertically, including:

- as a solar fence to enclose properties and buildings and produce solar energy at the same time (Figure 15a);
- as noise barriers to reduce noise levels between noise sources and receivers (Figure 15b); and

- as a building-integrated photovoltaic (BIPV) system by integrating bPV modules into the building envelope, such as the roof or façade (Figure 15c).



Figure 15. Bifacial photovoltaic modules placed vertically as a solar fence (a) [107], noise barrier (b) [118], and integrated building PV (c) [119].

The photovoltaic fences serve as protective shields for properties by applying bifacial photovoltaic modules vertically as fences. In some cases, such as in Hitachi (Japan) [120], it is possible to generate electrical energy even equivalent to the fixed south-facing mono-PV with an optimal inclination. Additionally, it can be installed regardless of the azimuth angle of the protected building [121]. Furthermore, replacing south-facing monofacial modules with bifacial in solar fences can improve the electrical output by up to 150%, making this application more suitable for bPV technology [122].

The bPV vertical noise barriers in roads can also be a very good synergistic application, due to the high energy output for any road orientation, which is not the case for conventional mono-PV modules. However, the use of bifacial photovoltaic modules as a noise barrier requires an increase in the thickness of the module to be able to absorb noise and withstand any stones the car's wheels might launch, which can cast a shadow on the rear face of the bifacial module. This can reduce the energy yield of about 3% [123]. Two solutions can be considered to reduce the losses due to shading: placing the bifacial module cells away from the module frame or adding more bypass diodes [124].

The installation of building-integrated photovoltaic BIPV modules is a growing domain, as they allow the production of energy locally and the replacement of conventional building materials, resulting in reduced construction costs and increased energy autonomy. Bifacial photovoltaic modules might be more suitable in this application due to the characteristic of interception of rear and front lights. In [125], a bPV glass-glass facade could increase the energy performance of the building by about 5% more than mono-PV. It can serve as thermal insulation and a noise barrier to the building [126]. They are less sensitive to snow and dust than an optimal sloped installation, so they are cleaner, thus reducing soiling losses and cleaning costs [126]. In addition, the effect of orientation is less severe than that of conventional monofacial PV modules [127]. An installations example using the bifacial photovoltaic module as a solar fence and noise barrier is listed in Table 3.

Table 3. Examples of installations of solar fences and noise barriers with bifacial photovoltaic modules.

	No	Location	Capacity	Further Information	Reference
Solar Fence	1	St. Martin bei Lofer, Austria	52.55 kWp	This solar fence serves as an enclosure for the chicken farm and for the self-consumption of energy, with a yield of 50 MWh/year.	[107]
	2	Maishofen, Austria	3.42 kWp	The solar fence serves as a housing enclosure and for self-consumption of energy, with a yield of 3500 KWh/year.	[107]
Noise barriers	4	Switzerland, Zürich, Aurugg	10 kWp	The first bifacial PV noise barrier in the world.	[128]
	5	Delhi, India	100 kWp	Noise barriers bifacial vertical panels for the Delhi Metro.	[129]

5. Conclusions

Bifacial technology is growing in importance in the PV industry and is expected to dominate it with a 70% share in 2030. The primary cause of this dominance is the increase in energy output brought on by receiving irradiance from both sides. This advantage, however, is highly dependent on a number of factors, such as ground reflectance, clearance, as well as tilt and orientation. Bifacial technology can produce a lower LCOE than traditional PV technology under optimal conditions. One of the main challenges of bPV technology is the characterization of bPV modules. In order to facilitate the market's wide adoption of bifacial PV, a bifacial standard is needed, to help manufacturers in various parts of the world to fairly and globally market their products. In general, this operation has always been performed under standard bPV conditions, which provide unreliable results for the characteristics and the development of the technology. The current market requires standard bPV test conditions adapted to both sides of the module, especially the rear side. In addition, the spectral irradiance of the backside tests must be unified, which was not the case for monofacial systems due to the neglected effect of ground-reflected irradiance on monofacial performance. The spectral albedo of the light soil can be adopted to unify the back reflected irradiance. Different models are available in the literature to predict the performance of bPV systems but in this paper, we see that all of the thermal simulation models are derived from the monofacial model. A closer comprehension of thermal behavior will advance the development of bPV technology. Additionally, combining the models with the device structure to analyze the influence of the latter on the model parameters can improve the accuracy of these models. The economic competitiveness of the technology is another challenge that may limit its expansion in the market. However, the application of bPV technology in suitable applications has shown promising results, whether in agrivoltaics with simultaneous land use between agriculture and PV modules, or in aquavoltaics, placing the modules on a water surface, or in vertical applications such as building-integrated PV, or solar fences. Further research can be performed to examine the implementation options and to concretize the benefits of adopting this technology in order to better comprehend the various applications of bifacial photovoltaics.

Author Contributions: E.M.: Conceptualization, Methodology, Software, Validation, Investigation, Data Curation, Writing—Original Draft, Writing—Review and Editing. L.M.: Investigation, Methodology, Supervision, Writing—original draft, Writing—review and editing. F.M.A.: Investigation, Methodology, Supervision, Writing—review and editing, Funding acquisition—E.F.F.: Conceptualization, Investigation, Methodology, Supervision, Writing—review and editing, Funding acquisition. All authors have read and agreed to the published version of the manuscript.

Funding: This research has been partially funded by the project “UltraMicroCPV” (MICINN-Agencia Estatal de Investigación: PID2019-106497RB-I00/AEI/10.13039/501100011033) and by the project NACe-CPV/TE (Junta de Andalucía, PAIDI 2020: P18-RT-1595). Elmehdi Mouhib is supported by the Spanish Ministry of Science and Innovation under the program “ayudas para contratos predoctorales para la formación de doctores (FPI)” (Ref: PRE2020-092077). Eduardo F. Fernández also thanks the Agencia Estatal de Investigación for the funds received under the “Ramón y Cajal Programme” (RYC-2017-21910). L. Micheli’s work was supported by Sole4PV, a project funded by the Italian Ministry of University and Research under the 2019 «Rita Levi Montalcini» Program for Young Researchers.

Data Availability Statement: Not applicable.

Conflicts of Interest: The authors declare that they have no known competing financial interests or personal relationships that could have appeared to influence the work reported in this paper.

Nomenclature

Abbreviations

bPV	Bifacial Photovoltaic
mono PV	Monofacial Photovoltaic
LCOE	Levelized Cost of Energy
BOS	Balance of System
AR	Anti-reflective
ARC	Antireflection Coating
IR	Infrared
PERC	Passivated Emitter Back Contact
PERL	Passivated Emitter Back Contact with Local Diffusion
PERT	Passivated Emitter Back Contact with Full Diffusion
HIT	Heterojunction, intrinsic thin film
IBC	Interdigitated Back Contact
DSBCSC	Double-side buried contact
EVA	Ethylene-Vinyl Acetate copolymer
C-Si	Crystalline Silicon
BSF	Back Surface Field
BG	Bifacial Gain
GHI	Global Horizontal Irradiance
AM	Air Mass
FF	Fill Factor
STC	Standard Test Conditions
SEM	Single Exponential Model
APV	Agrivoltaic
CPV	Concentrator Photovoltaic
PAR	Photosynthetically Active Radiation ($\mu\text{moL m}^{-2} \text{s}^{-1}$)
LCP	Light Compensation Point
LSP	Light Saturation Point
LER	Land Equivalence Ratio
LPF	Light Productivity Factor
ST	Solar Tracking
RT	Reverse Tracking
CT	Customized Tracking
FPV	Floating Photovoltaic
BIPV	Building Integrated Photovoltaic

Symbols

J_{sc}	Short-circuit Current Density (A/m^2)
V_{oc}	Open Circuit Voltage (V)
P_m	Power (W)
η	Power Conversion Efficiency
$\eta_{stc}^{F,R}$	Power Conversion Efficiency for the Front/Rear in STC conditions
Superscripts F and R	Front Side and Rear Side
φ	Bifaciality Factor
Y	Energy Yield (KWh)
$Y_{bifacial}$	Bifacial Energy Yield (KWh)
$Y_{monofacial}$	Monofacial Energy Yield (KWh)
G^{Front}	Front Irradiance (W/m^2)
G^{Rear}	Rear Irradiance (W/m^2)
G_T	Sum of G^{Front} and
SR	Spectral Response (A/W)
α	Ground Albedo
A_r	Spectral Reflectivity
G_b	Beam Irradiance on a Horizontal Surface
R_b	Ratio of Beam Radiation on the Tilted Surface to Horizontal
$G_{d,tilt}$	Total Tilted Diffuse Irradiance

G_d	Diffuse Horizontal Irradiance
β	Photovoltaic Module Tilt Angle
F1	Circumsolar Brightness Coefficient
F2	Horizon Brightness Coefficient
θ_z	Sun Zenith Angle
ϵ	Sky Clearness Index
Δ	Brightness Index
L	Photovoltaic Modules Length (m)
h	Module-to-Ground Clearance (m)
F_{Sky}^{Rear}	Module to Sky View Factor
$F_{unshaded\ ground}^{Rear}$	Module to Unshaded Ground View Factor
$F_{shaded\ ground}^{Rear}$	Module to Shaded Ground View Factor
P_{PV}	Total Output Power
T	Temperature (K)
β_T	Temperature Coefficient (%/°C)
P_{mpp}	Output Power at the Maximum Power Point
R_S	Series Resistance
R_P	Shunt Resistance
G_e	Bifacial Equivalent Irradiance
E_g	Band Gap Energy
q	Electric Charge (1.6×10^{-19} C)
T_a	Ambient Temperature (°C)
T_{NOCT}	Nominal Operating Cell Temperature (°C)
G_{ref}	Irradiance under STC (1000 W/m ²)
ΔT	Temperature Difference (°C)
T_m	Module Temperature (°C)
U_0	Constant Heat Transfer Coefficient (W/m ² K)
U_1	Convective Heat Transfer Component (W/m ³ sK)
U_w	Wind Speed (m/s)
$C_{p,PV}$	Specific Heat of the PV Layer (J/(kg K))
δ_{PV}	Thickness of the PV Layer (m)
ρ_{PV}	Density of the PV Layer (kg/m ³)
τ_g	Glass Transitivity (%)
T_{EVA2}	Lower EVA Temperature (K)
$R_{PV-EVA2}$	Conductive Thermal Resistance Between PV Layer and Lower EVA (K/W)
P_n	Net Photosynthetic Rate
θ_{AOI}	Angle of Incidence
I_{PV}	Electrical Energy Produced by the Bifacial Modules
G_{GR}	Global Ground Irradiance (W/m ²)
PAR_{th}	Saturation Photosynthesis Active Radiation ($\mu\text{moL m}^{-2} \text{s}^{-1}$)
Y_{PAR}	Yield for a Precise Photosynthetically Active Radiation

References

1. Kreinin, L.; Bordin, N.; Karsenty, A.; Drori, A.; Eisenberg, N. Experimental Analysis of the Increases in Energy Generation of Bifacial over Mono-Facial Pv Modules. In Proceedings of the 26th European Photovoltaic Solar Energy Conference and Exhibition, Hambourg, Germany, 5–9 September 2011; pp. 3140–3143.
2. Hiroshi, M. Radiation Energy Transducing Device. U.S. Patent US3278811A, 3 October 1961.
3. Cuevas, A.; Luque, A.; Eguren, J.; del Alamo, J. 50 Per Cent More Output Power from an Albedo-Collecting Flat Panel Using Bifacial Solar Cells. *Sol. Energy* **1982**, *29*, 419–420. [[CrossRef](#)]
4. Kasahara, N.; Yoshioka, K.; Saitoh, T. Performance Evaluation of Bifacial Photovoltaic Modules for Urban Application. In Proceedings of the 3rd World Conference on Photovoltaic Energy Conversion, Osaka, Japan, 11–18 May 2003; Volume C, pp. 2455–2458.
5. Liang, T.S.; Pravettoni, M.; Deline, C.; Stein, J.S.; Kopecek, R.; Singh, J.P.; Luo, W.; Wang, Y.; Aberle, A.G.; Khoo, Y.S. A Review of Crystalline Silicon Bifacial Photovoltaic Performance Characterisation and Simulation. *Energy Environ. Sci.* **2019**, *12*, 116–148. [[CrossRef](#)]
6. Kopecek, R.; Libal, J. Bifacial Photovoltaics 2021: Status, Opportunities and Challenges. *Energies* **2021**, *14*, 2076. [[CrossRef](#)]
7. Dullweber, T.; Schmidt, J. Industrial Silicon Solar Cells Applying the Passivated Emitter and Rear Cell (PERC) Concept—A Review. *IEEE J. Photovolt.* **2016**, *6*, 1366–1381. [[CrossRef](#)]

8. Deline, C.A.; Ayala Pelaez, S.; Marion, W.F.; Sekulic, W.R.; Woodhouse, M.A.; Stein, J. *Bifacial PV System Performance: Separating Fact from Fiction*; National Renewable Energy Lab.(NREL): Golden, CO, USA, 2019.
9. Muehleisen, W.; Loeschnig, J.; Feichtner, M.; Burgers, A.R.R.; Bende, E.E.E.; Zamini, S.; Yerasimou, Y.; Kosel, J.; Hirschl, C.; Georghiou, G.E.E. Energy Yield Measurement of an Elevated PV System on a White Flat Roof and a Performance Comparison of Monofacial and Bifacial Modules. *Renew. Energy* **2021**, *170*, 613–619. [[CrossRef](#)]
10. Rodriguez-Gallegos, C.D.; Bieri, M.; Gandhi, O.; Singh, J.P.; Reindl, T.; Panda, S.K.K. Monofacial vs Bifacial Si-Based PV Modules: Which One Is More Cost-Effective? *Sol. Energy* **2018**, *176*, 412–438. [[CrossRef](#)]
11. Tina, G.M.; Bontempo Scavo, F.; Merlo, L.; Bizzarri, F. Comparative Analysis of Monofacial and Bifacial Photovoltaic Modules for Floating Power Plants. *Appl. Energy* **2021**, *281*, 116084. [[CrossRef](#)]
12. Yin, H.P.P.; Zhou, Y.F.F.; Sun, S.L.L.; Tang, W.S.S.; Shan, W.; Huang, X.M.M.; Shen, X.D.D. Optical Enhanced Effects on the Electrical Performance and Energy Yield of Bifacial PV Modules. *Sol. Energy* **2021**, *217*, 245–252. [[CrossRef](#)]
13. Hubner, A.; Aberle, A.; Hezel, R. Temperature Behavior of Monofacial and Bifacial Silicon Solar Cells. In Proceedings of the Conference Record of the Twenty Sixth IEEE Photovoltaic Specialists Conference, Anaheim, CA, USA, 29 September–3 October 1997; pp. 223–226.
14. Ishikawa, S.N. World First Large Scale 1.25 MW Bifacial PV Power Plant on Snowy Area in Japan. In Proceedings of the 3rd bifi PV Workshop, Miyazaki, Japan, 29–30 September 2016.
15. Reuters Events Renewables Giant Bifacial PV Plants Act as Springboard for Growth. Available online: <https://analysis.newenergyupdate.com/pv-insider/giant-bifacial-pv-plants-act-springboard-growth> (accessed on 18 January 2022).
16. Burnham, L.; Riley, D.; Walker, B.; Pearce, J.M. Performance of Bifacial Photovoltaic Modules on a Dual-Axis Tracker in a High-Latitude, High-Albedo Environment. In Proceedings of the 2019 IEEE 46th Photovoltaic Specialists Conference (PVSC), Chicago, IL, USA, 16–21 June 2019; pp. 1320–1327.
17. Liu, B.Y.H.; Jordan, R.C. The Long-Term Average Performance of Flat-Plate Solar-Energy Collectors. *Sol. Energy* **1963**, *7*, 53–74. [[CrossRef](#)]
18. Duffie, J.A.; Beckman, W.A. *Solar Engineering of Thermal Processes*, 3rd ed.; Wiley: Hoboken, NJ, USA, 1982; Volume 3.
19. Katsikogiannis, O.A.; Ziar, H.; Isabella, O. Integration of Bifacial Photovoltaics in Agrivoltaic Systems: A Synergistic Design Approach. *Appl. Energy* **2022**, *309*, 118475. [[CrossRef](#)]
20. Assoa, Y.B.; Thony, P.; Messaoudi, P.; Schmitt, E.; Bizzini, O.; Gelibert, S.; Therme, D.; Rudy, J.; Chabuel, F. Study of a Building Integrated Bifacial Photovoltaic Facade. *Sol. Energy* **2021**, *227*, 497–515. [[CrossRef](#)]
21. Pringle, A.M.; Handler, R.M.M.; Pearce, J.M.M. Aquavoltaics: Synergies for Dual Use of Water Area for Solar Photovoltaic Electricity Generation and Aquaculture. *Renew. Sustain. Energy Rev.* **2017**, *80*, 572–584. [[CrossRef](#)]
22. Gu, W.; Ma, T.; Song, A.; Li, M.; Shen, L. Mathematical Modelling and Performance Evaluation of a Hybrid Photovoltaic-Thermoelectric System. *Energy Convers. Manag.* **2019**, *198*, 111800. [[CrossRef](#)]
23. Raina, G.; Sinha, S. A Simulation Study to Evaluate and Compare Monofacial Vs Bifacial PERC PV Cells and the Effect of Albedo on Bifacial Performance. *Mater. Today Proc.* **2020**, *46*, 5242–5247. [[CrossRef](#)]
24. Wang, A.; Xuan, Y. A Detailed Study on Loss Processes in Solar Cells. *Energy* **2018**, *144*, 490–500. [[CrossRef](#)]
25. Chantana, J.; Horio, Y.; Kawano, Y.; Hishikawa, Y.; Minemoto, T. Spectral Mismatch Correction Factor for Precise Outdoor Performance Evaluation and Description of Performance Degradation of Different-Type Photovoltaic Modules. *Sol. Energy* **2019**, *181*, 169–177. [[CrossRef](#)]
26. Dupré, O.; Vaillon, R.; Green, M.A. A Full Thermal Model for Photovoltaic Devices. *Sol. Energy* **2016**, *140*, 73–82. [[CrossRef](#)]
27. Dupré, O. *Physics of the Thermal Behavior of Photovoltaic Devices*; INSA de Lyon: Villeurbanne, France, 2015.
28. Tang, H.B.B.; Ma, S.; Lv, Y.; Li, Z.P.P.; Shen, W.Z.Z. Optimization of Rear Surface Roughness and Metal Grid Design in Industrial Bifacial PERC Solar Cells. *Sol. Energy Mater. Sol. Cells* **2020**, *216*, 110712. [[CrossRef](#)]
29. Rabanal-Arabach, J.; Schneider, A. Anti-Reflective Coated Glass and Its Impact on Bifacial Modules' Temperature in Desert Locations. *Energy Procedia* **2016**, *92*, 590–599. [[CrossRef](#)]
30. Saive, R.; Russell, T.C.R.R.; Atwater, H.A. Enhancing the Power Output of Bifacial Solar Modules by Applying Effectively Transparent Contacts (ETCs) With Light Trapping. *IEEE J. Photovolt.* **2018**, *8*, 1183–1189. [[CrossRef](#)]
31. Sepeai, S.; Sulaiman, M.Y.; Sopian, K.; Zaidi, S.H. Investigation of Back Surface Fields Effect on Bifacial Solar Cells. In *AIP Conference Proceedings*; American Institute of Physics: College Park, MD, USA, 2012; Volume 1502, pp. 322–335.
32. Moehlecke, A.; Zanesco, I.; Luque, A. Practical High Efficiency Bifacial Solar Cells. In Proceedings of the 1994 IEEE 1st World Conference on Photovoltaic Energy Conversion—WCPEC (A Joint Conference of PVSC, PVSEC and PSEC), Waikoloa, HI, USA, 5–9 December 1994; Volume 2, pp. 1663–1666.
33. Shoukry, I.; Libal, J.; Kopecek, R.; Wefringhaus, E.; Werner, J. Modelling of Bifacial Gain for Stand-Alone and in-Field Installed Bifacial PV Modules. *Energy Procedia* **2016**, *92*, 600–608. [[CrossRef](#)]
34. Stein, J.S.; Reise, C.; Castro, J.B.; Friesen, G.; Maugeri, G.G.; Urrejola, E.E.; Ranta, S. *Bifacial Photovoltaic Modules and Systems: Experience and Results from International Research and Pilot Applications*; Sandia National Lab.(SNL-NM): Albuquerque, NM, USA; Livermore, CA, USA, 2021.
35. Spectral Response. In *Encyclopedia of Microfluidics and Nanofluidics*; Springer: Boston, MA, USA, 2008; p. 1881.

36. Gostein, M.; Marion, B.; Stueve, B. Spectral Effects in Albedo and Rearside Irradiance Measurement for Bifacial Performance Estimation. In Proceedings of the 2020 47th IEEE Photovoltaic Specialists Conference (PVSC), Calgary, AB, Canada, 15 June–21 August 2020; Volume 2020-June, pp. 515–519.
37. Brennan, M.P.P.; Abramase, A.L.L.; Andrews, R.W.W.; Pearce, J.M.M. Effects of Spectral Albedo on Solar Photovoltaic Devices. *Sol. Energy Mater. Sol. Cells* **2014**, *124*, 111–116. [CrossRef]
38. Myers, D.R.; Gueymard, C.A. Description and Availability of the SMARTS Spectral Model for Photovoltaic Applications. In *Organic Photovoltaics V*; Kafafi, Z.H., Lane, P.A., Eds.; SPIE: Bellingham, WA, USA, 2004; Volume 5520, p. 56.
39. Khoo, Y.S.; Nobre, A.; Malhotra, R.; Yang, D.; Ruther, R.; Reindl, T.; Aberle, A.G. Optimal Orientation and Tilt Angle for Maximizing In-Plane Solar Irradiation for PV Applications in Singapore. *IEEE J. Photovolt.* **2014**, *4*, 647–653. [CrossRef]
40. Liu, B.; Jordan, R. Daily Insolation on Surfaces Tilted towards Equator. *ASHRAE J.* **1961**, *10*, 53–59.
41. Temps, R.C.; Coulson, K.L.L. Solar Radiation Incident upon Slopes of Different Orientations. *Sol. Energy* **1977**, *19*, 179–184. [CrossRef]
42. Perez, R.; Seals, R.; Ineichen, P.; Stewart, R.; Menicucci, D. A New Simplified Version of the Perez Diffuse Irradiance Model for Tilted Surfaces. *Sol. Energy* **1987**, *39*, 221–231. [CrossRef]
43. Iqbal, M. *An Introduction to Solar Radiation*; Elsevier: Amsterdam, The Netherlands, 1983; ISBN 9780123737502.
44. Gueymard, C.A.; Lara-Fanego, V.; Sengupta, M.; Xie, Y. Surface Albedo and Reflectance: Review of Definitions, Angular and Spectral Effects, and Intercomparison of Major Data Sources in Support of Advanced Solar Irradiance Modeling over the Americas. *Sol. Energy* **2019**, *182*, 194–212. [CrossRef]
45. Sandia National Laboratories. POA Ground Reflected. Available online: <https://pvpmc.sandia.gov/modeling-steps/1-weather-design-inputs/plane-of-array-poa-irradiance/calculating-poa-irradiance/poa-ground-reflected/> (accessed on 1 November 2022).
46. Suri, T.C.M. SOLARGIS. Available online: <https://solargis.com/> (accessed on 1 November 2022).
47. Meteotest Switzerland Meteonorm Software 7. Available online: <http://www.meteonorm.com/> (accessed on 1 November 2022).
48. PVGIS Photovoltaic Geographical Information System. Available online: http://re.jrc.ec.europa.eu/pvg_download/map_index.html%0Ahttps://re.jrc.ec.europa.eu/pvg_tools/en/%0Ahttps://re.jrc.ec.europa.eu/pvg_tools/es/#PVP%0Ahttps://ec.europa.eu/jrc/en/pvgis (accessed on 1 November 2022).
49. Appelbaum, J. The Role of View Factors in Solar Photovoltaic Fields. *Renew. Sustain. Energy Rev.* **2018**, *81*, 161–171. [CrossRef]
50. PV Performance Modeling Collaborative | Ray Tracing Models for Backside Irradiance. Available online: <https://pvpmc.sandia.gov/pv-research/bifacial-pv-project/bifacial-pv-performance-models/ray-tracing-models-for-backside-irradiance/> (accessed on 1 November 2022).
51. Radiance Software. Available online: <https://floyd.lbl.gov/radiance/framed.html> (accessed on 28 March 2022).
52. Trace PRO Software. Available online: <https://lambdares.com/tracepro/> (accessed on 28 March 2022).
53. Comsol Software. Available online: <https://www.comsol.com/ray-optics-module> (accessed on 28 March 2022).
54. Libal, J.; Kopecek, R. *Bifacial Photovoltaics: Technology, Applications and Economics*; Libal, J., Kopecek, R., Eds.; Institution of Engineering and Technology: Stevenage, UK, 2018; ISBN 9781785612749.
55. Pelaez, S.A.; Deline, C.; MacAlpine, S.M.; Marion, B.; Stein, J.S.; Kostuk, R.K. Comparison of Bifacial Solar Irradiance Model Predictions With Field Validation. *IEEE J. Photovolt.* **2019**, *9*, 82–88. [CrossRef]
56. Castillo-Aguilella, J.E.; Hauser, P.S. Bifacial Photovoltaic Module Best-Fit Annual Energy Yield Model with Azimuthal Correction. In Proceedings of the IEEE 44th Photovoltaic Specialists Conference (PVSC 2017), Washington, DC, USA, 25–30 June 2017; pp. 195–197.
57. Gu, W.; Ma, T.; Ahmed, S.; Zhang, Y.; Peng, J. A Comprehensive Review and Outlook of Bifacial Photovoltaic (BPV) Technology. *Energy Convers. Manag.* **2020**, *223*, 113283. [CrossRef]
58. Tossa, A.K.; Soro, Y.M.M.; Azoumah, Y.; Yamagueu, D. A New Approach to Estimate the Performance and Energy Productivity of Photovoltaic Modules in Real Operating Conditions. *Sol. Energy* **2014**, *110*, 543–560. [CrossRef]
59. Ma, J.; Man, K.L.; Ting, T.O.; Zhang, N.; Guan, S.-U.U.; Wong, P.W.H.H. Approximate Single-Diode Photovoltaic Model for Efficient I–V Characteristics Estimation. *Sci. World J.* **2013**, *2013*, 1–7. [CrossRef]
60. Ross, R.G., Jr. Design Tech for FP PV Arrays. 1981. Available online: https://www2.jpl.nasa.gov/adv_tech/photovol/ppr_81-8-5/Design%20Tech%20for%20FP%20PV%20Arrays_PVSC1981.pdf (accessed on 1 November 2022).
61. Leonardi, M.; Corso, R.; Milazzo, R.G.; Connelli, C.; Foti, M.; Gerardi, C.; Bizzarri, F.; Privitera, S.M.S.S.; Lombardo, S.A. The Effects of Module Temperature on the Energy Yield of Bifacial Photovoltaics: Data and Model. *Energies* **2021**, *15*, 22. [CrossRef]
62. Hassanian, R.; Riedel, M.; Yeganeh, N. A Review in Context to Wind Effect on NOCT Model for Photovoltaic Panel. *Crimson Publ. Wings to Res.* **2022**, *2*, 1–3.
63. King, D.L.; Boyson, W.E.; Kratochvil, J.A.; Boyson, W.E.; King, D.L. *Photovoltaic Array Performance Model*; Sandia National Laboratories (SNL): Albuquerque, NM, USA; Livermore, CA, USA, 2004; Volume 8.
64. PVPerformance Sandia Module Temperature Model. Available online: <https://pvpmc.sandia.gov/modeling-steps/2-dc-module-iv/module-temperature/sandia-module-temperature-model/> (accessed on 23 May 2022).
65. Faiman, D. Assessing the Outdoor Operating Temperature of Photovoltaic Modules. *Prog. Photovolt. Res. Appl.* **2008**, *16*, 307–315. [CrossRef]

66. Gu, W.; Ma, T.; Li, M.; Shen, L.; Zhang, Y. A Coupled Optical-Electrical-Thermal Model of the Bifacial Photovoltaic Module. *Appl. Energy* **2020**, *258*, 114075. [[CrossRef](#)]
67. Tina, G.M.; Scavo, F.B.; Gagliano, A. Multilayer Thermal Model for Evaluating the Performances of Monofacial and Bifacial Photovoltaic Modules. *IEEE J. Photovolt.* **2020**, *10*, 1035–1043. [[CrossRef](#)]
68. Barron-Gafford, G.A.; Pavao-Zuckerman, M.A.; Minor, R.L.; Sutter, L.F.; Barnett-Moreno, I.; Blackett, D.T.; Thompson, M.; Dimond, K.; Gerlak, A.K.; Nabhan, G.P.; et al. Agrivoltaics Provide Mutual Benefits across the Food–Energy–Water Nexus in Drylands. *Nat. Sustain.* **2019**, *2*, 848–855. [[CrossRef](#)]
69. Dupraz, C.; Marrou, H.; Talbot, G.; Dufour, L.; Nogier, A.; Ferard, Y. Combining Solar Photovoltaic Panels and Food Crops for Optimising Land Use: Towards New Agrivoltaic Schemes. *Renew. Energy* **2011**, *36*, 2725–2732. [[CrossRef](#)]
70. Sato, D.; Yamada, N. Design and Testing of Highly Transparent Concentrator Photovoltaic Modules for Efficient Dual-land-use Applications. *Energy Sci. Eng.* **2020**, *8*, 779–788. [[CrossRef](#)]
71. Domínguez, C.; Jost, N.; Askins, S.; Victoria, M.; Antón, I. A Review of the Promises and Challenges of Micro-Concentrator Photovoltaics. In *AIP Conference Proceedings*; AIP Publishing LLC: Melville, NY, USA, 2017; Volume 1881, p. 080003.
72. Thompson, E.P.; Bombelli, E.L.; Shubham, S.; Watson, H.; Everard, A.; D’Ardes, V.; Schievano, A.; Bocchi, S.; Zand, N.; Howe, C.J.; et al. Tinted Semi-Transparent Solar Panels Allow Concurrent Production of Crops and Electricity on the Same Cropland. *Adv. Energy Mater.* **2020**, *10*, 2001189. [[CrossRef](#)]
73. Zhi, L.; Yano, A.; Marco, C.; Yoshioka, H.; Kita, I.; Ibaraki, Y. Shading and Electric Performance of a Prototype Greenhouse Blind System Based on Semi-Transparent Photovoltaic Technology. *J. Agric. Meteorol.* **2018**, *74*, 114–122. [[CrossRef](#)]
74. Distler, A.; Brabec, C.J.; Egelhaaf, H.J. Organic Photovoltaic Modules with New World Record Efficiencies. *Prog. Photovolt. Res. Appl.* **2021**, *29*, 24–31. [[CrossRef](#)]
75. Öner, İ.V. Operational Stability and Degradation of Organic Solar Cells. *Period. Eng. Nat. Sci.* **2017**, *5*. [[CrossRef](#)]
76. Evans, J.R. Improving Photosynthesis. *Plant Physiol.* **2013**, *162*, 1780–1793. [[CrossRef](#)]
77. Teskey, R.O.; Sheriff, D.W.; Hollinger, D.Y.; Thomas, R.B. External and Internal Factors Regulating Photosynthesis. In *Resource Physiology of Conifers*; Elsevier: Amsterdam, The Netherlands, 1995; pp. 105–140. ISBN 9780126528701.
78. Maire, V.; Wright, I.J.; Prentice, I.C.; Batjes, N.H.; Bhaskar, R.; van Bodegom, P.M.; Cornwell, W.K.; Ellsworth, D.; Niinemets, Ü.; Ordonez, A.; et al. Global Effects of Soil and Climate on Leaf Photosynthetic Traits and Rates. *Glob. Ecol. Biogeogr.* **2015**, *24*, 706–717. [[CrossRef](#)]
79. LEACH, J.E. Some Effects of Air Temperature and Humidity on Crop and Leaf Photosynthesis, Transpiration and Resistance to Gas Transfer. *Ann. Appl. Biol.* **1979**, *92*, 287–297. [[CrossRef](#)]
80. Kuo, J.; den Hartog, C. Seagrass Taxonomy and Identification Key. In *Global Seagrass Research Methods*; Elsevier: Amsterdam, The Netherlands, 2001; pp. 31–58.
81. Runkle, B.E. *Interactions of Light, CO₂ and Temperature on Photosynthesis*; GNP; Michigan State University: East Lansing, MI, USA, 2015; Volume 2015.
82. Hartzell, S.; Bartlett, M.S.; Porporato, A. Unified Representation of the C₃, C₄, and CAM Photosynthetic Pathways with the Photo3 Model. *Ecol. Modell.* **2018**, *384*, 173–187. [[CrossRef](#)]
83. Yin, X.; Struik, P.C.C. C₃ and C₄ Photosynthesis Models: An Overview from the Perspective of Crop Modelling. *NJAS Wagening. J. Life Sci.* **2009**, *57*, 27–38. [[CrossRef](#)]
84. Mahendra, S.; Ogren, W.L.; Widholm, J.M. Photosynthetic Characteristics of Several C₃ and C₄ Plant Species Grown Under Different Light Intensities 1. *Crop Sci.* **1974**, *14*, 563–566. [[CrossRef](#)]
85. Weselek, A.; Bauerle, A.; Hartung, J.; Zikeli, S.; Lewandowski, I.; Högy, P. Agrivoltaic System Impacts on Microclimate and Yield of Different Crops within an Organic Crop Rotation in a Temperate Climate. *Agron. Sustain. Dev.* **2021**, *41*, 59. [[CrossRef](#)]
86. Marrou, H.; Guilioni, L.; Dufour, L.; Dupraz, C.; Wery, J. Microclimate under Agrivoltaic Systems: Is Crop Growth Rate Affected in the Partial Shade of Solar Panels? *Agric. For. Meteorol.* **2013**, *177*, 117–132. [[CrossRef](#)]
87. Marrou, H.; Dufour, L.; Wery, J. How Does a Shelter of Solar Panels Influence Water Flows in a Soil–Crop System? *Eur. J. Agron.* **2013**, *50*, 38–51. [[CrossRef](#)]
88. Othman, N.F.; Ya’acob, M.E.; Abdul-Rahim, A.S.; Hizam, H.; Farid, M.M.; Abd Aziz, S. Inculcating Herbal Plots as Effective Cooling Mechanism in Urban Planning. *Acta Hortic.* **2017**, *1152*, 235–242. [[CrossRef](#)]
89. Patel, B.; Gami, B.; Baria, V.; Patel, A.; Patel, P. Co-Generation of Solar Electricity and Agriculture Produce by Photovoltaic and Photosynthesis—Dual Model by Abellon, India. *J. Sol. Energy Eng.* **2019**, *141*, 1–9. [[CrossRef](#)]
90. NREL Benefits of Agrivoltaics Across the Food-Energy-Water Nexus. Available online: <https://www.nrel.gov/news/program/2019/benefits-of-agrivoltaics-across-the-food-energy-water-nexus.html> (accessed on 9 June 2022).
91. Al-Saidi, M.; Lahham, N. Solar Energy Farming as a Development Innovation for Vulnerable Water Basins. *Dev. Pract.* **2019**, *29*, 619–634. [[CrossRef](#)]
92. Imran, H.; Riaz, M.H. Investigating the Potential of East/West Vertical Bifacial Photovoltaic Farm for Agrivoltaic Systems. *J. Renew. Sustain. Energy* **2021**, *13*, 033502. [[CrossRef](#)]
93. Sekiyama, T.; Nagashima, A. Solar Sharing for Both Food and Clean Energy Production: Performance of Agrivoltaic Systems for Corn, A Typical Shade-Intolerant Crop. *Environments* **2019**, *6*, 65. [[CrossRef](#)]
94. Lytle, W.; Meyer, T.K.; Tanikella, N.G.; Burnham, L.; Engel, J.; Schelly, C.; Pearce, J.M. Conceptual Design and Rationale for a New Agrivoltaics Concept: Pasture-Raised Rabbits and Solar Farming. *J. Clean. Prod.* **2021**, *282*, 124476. [[CrossRef](#)]

95. Tahir, Z.; Butt, N.Z. Implications of Spatial-Temporal Shading in Agrivoltaics under Fixed Tilt & Tracking Bifacial Photovoltaic Panels. *Renew. Energy* **2022**, *190*, 167–176. [CrossRef]
96. Riaz, M.H.; Imran, H.; Alam, H.; Alam, M.A.; Butt, N.Z.; Ashraful, M. Crop-Specific Optimization of Bifacial PV Arrays for Agrivoltaic Food-Energy Production: The Light-Productivity-Factor Approach. *IEEE J. Photovolt.* **2022**, *12*, 572–580. [CrossRef]
97. Campana, P.E.; Stridh, B.; Amaducci, S.; Colauzzi, M. Optimisation of Vertically Mounted Agrivoltaic Systems. *J. Clean. Prod.* **2021**, *325*, 129091. [CrossRef]
98. Weselek, A.; Ehmann, A.; Zikeli, S.; Lewandowski, I.; Schindeler, S.; Högy, P. Agrophotovoltaic Systems: Applications, Challenges, and Opportunities. A Review. *Agron. Sustain. Dev.* **2019**, *39*, 35. [CrossRef]
99. Dinesh, H.; Pearce, J.M. The Potential of Agrivoltaic Systems. *Renew. Sustain. Energy Rev.* **2016**, *54*, 299–308. [CrossRef]
100. Imran, H.; Riaz, M.H.; Butt, N.Z. Optimization of Single-Axis Tracking of Photovoltaic Modules for Agrivoltaic Systems. In Proceedings of the 2020 47th IEEE Photovoltaic Specialists Conference (PVSC), Calgary, AB, Canada, 15 June–21 August 2020; Volume 2020-June, pp. 1353–1356.
101. Ullah, A.; Imran, H.; Maqsood, Z.; Butt, N.Z. Investigation of Optimal Tilt Angles and Effects of Soiling on PV Energy Production in Pakistan. *Renew. Energy* **2019**, *139*, 830–843. [CrossRef]
102. Asgharzadeh, A.; Lubenow, T.; Sink, J.; Marion, B.; Deline, C.; Hansen, C.; Stein, J.; Toor, F. Analysis of the Impact of Installation Parameters and System Size on Bifacial Gain and Energy Yield of PV Systems. In Proceedings of the 2017 IEEE 44th Photovoltaic Specialist Conference (PVSC), Washington, DC, USA, 25–30 June 2017; pp. 3333–3338.
103. Riaz, M.H.; Younas, R.; Imran, H.; Alam, M.A.; Butt, N.Z.; Younas, R.; Alam, M.A.; Butt, N.Z. Module Technology for Agrivoltaics: Vertical Bifacial Versus Tilted Monofacial Farms. *IEEE J. Photovolt.* **2021**, *11*, 469–477. [CrossRef]
104. Riaz, M.H.; Imran, H.; Younas, R.; Butt, N.Z. The Optimization of Vertical Bifacial Photovoltaic Farms for Efficient Agrivoltaic Systems. *Sol. Energy* **2021**, *230*, 1004–1012. [CrossRef]
105. Riaz, M.H.; Imran, H.; Butt, N.Z. Optimization of PV Array Density for Fixed Tilt Bifacial Solar Panels for Efficient Agrivoltaic Systems. In Proceedings of the 2020 47th IEEE Photovoltaic Specialists Conference (PVSC), Calgary, AB, Canada, 15 June–21 August 2020; Volume 2020-June, pp. 1349–1352.
106. Hassanpour Adeh, E.; Selker, J.S.; Higgins, C.W. Remarkable Agrivoltaic Influence on Soil Moisture, Micrometeorology and Water-Use Efficiency. *PLoS ONE* **2018**, *13*, e0203256. [CrossRef]
107. Next2Sun Agrivoltaics. Available online: <https://www.next2sun.de/en/references/> (accessed on 22 June 2022).
108. Brohm, R.; Khanh, N.Q. *Dual Use Approaches for Solar Energy and Food Production—International Experience and Potentials for Vietnam*; Green Innovation and Development Centre (GreenID): Hanoi, Vietnam, 2018.
109. BELLINI, E. Agrivoltaics for Pear Orchards. Available online: <https://www.pv-magazine.com/2020/10/02/agrivoltaics-for-pear-orchards/> (accessed on 22 June 2022).
110. Beshilas, L. Floating Solar Photovoltaics Could Make a Big Splash in the USA. Available online: [https://www.nrel.gov/state-local-tribal/blog/posts/floating-solar-photovoltaics-could-make-a-big-splash-in-the-usa.html#:~{:text=A floating solar photovoltaic\(FPV, land or building rooftops}](https://www.nrel.gov/state-local-tribal/blog/posts/floating-solar-photovoltaics-could-make-a-big-splash-in-the-usa.html#:~{:text=A floating solar photovoltaic(FPV, land or building rooftops}) (accessed on 5 July 2022).
111. Sharma, P.; Muni, B.; Sen, D. Design Parameters of 10 KW Floating Solar Power Plant Conference. *Int. Adv. Res. J. Sci. Eng. Technol.* **2016**, *2*, 85–89. [CrossRef]
112. Rodrigues, I.S.; Ramalho, G.L.B.; Medeiros, P.H.A. Potential of Floating Photovoltaic Plant in a Tropical Reservoir in Brazil. *J. Environ. Plan. Manag.* **2020**, *63*, 2334–2356. [CrossRef]
113. Sahu, A.; Yadav, N.; Sudhakar, K. Floating Photovoltaic Power Plant: A Review. *Renew. Sustain. Energy Rev.* **2016**, *66*, 815–824. [CrossRef]
114. Ponce, V.M.; Lohani, A.K.; Huston, P.T. Surface Albedo and Water Resources: Hydroclimatological Impact of Human Activities. *J. Hydrol. Eng.* **1997**, *2*, 197–203. [CrossRef]
115. Ziar, H.; Prudon, B.; Lin, F.Y.; Roeffen, B.; Heijkoop, D.; Stark, T.; Teurlincx, S.; Senerpont Domis, L.; Goma, E.G.; Extebarria, J.G.; et al. Innovative Floating Bifacial Photovoltaic Solutions for Inland Water Areas. *Prog. Photovolt. Res. Appl.* **2021**, *29*, 725–743. [CrossRef]
116. Widayat, A.A.; Ma’arif, S.; Syahindra, K.D.; Fauzi, A.F.; Setiawan, E.A.; Adhi Setiawan, E. Comparison and Optimization of Floating Bifacial and Monofacial Solar PV System in a Tropical Region. In Proceedings of the 2020 9th International Conference on Power Science and Engineering (ICPSE), London, UK, 23–25 October 2020; pp. 66–70.
117. First Floating Solar Farm in Thailand with UBE. Available online: <https://www.baywa-re.es/en/company/news/details/first-floating-solar-farm-in-thailand-with-ube> (accessed on 12 July 2022).
118. SEAC Solar Noise Barriers. Available online: <https://www.mitrex.com/noise-barriers/> (accessed on 12 July 2022).
119. Building-Integrated PV. Available online: <https://a2-solar.com/en/building-integrated-pv/> (accessed on 12 July 2022).
120. Joge, T.; Araki, I.; Takaku, K.; Nakahara, H.; Eguchi, Y.; Tomita, T. Advanced Applications of Bifacial Solar Modelus. In Proceedings of the 3rd World Conference on Photovoltaic Energy Conversion, Osaka, Japan, 11–18 May 2003; Volume C, pp. 2451–2454.
121. Araki, I.; Tatsunokuchi, M.; Nakahara, H.; Tomita, T. Bifacial PV System in Aichi Airport-Site Demonstrative Research Plant for New Energy Power Generation. *Sol. Energy Mater. Sol. Cells* **2009**, *93*, 911–916. [CrossRef]
122. Joge, T.; Eguchi, Y.; Imazu, Y.; Araki, I.; Uematsu, T.; Matsukuma, K. Applications and Field Tests of Bifacial Solar Modules. In Proceedings of the Conference Record of the Twenty-Ninth IEEE Photovoltaic Specialists Conference, New Orleans, LA, USA, 19–24 May 2002; pp. 1549–1552.

123. de Jong, M.M.; van den Donker, M.N.; Verkuilen, S.; Folkerts, W. Self-Shading in Bifacial Photovoltaic Noise Barriers. In Proceedings of the 32nd European Photovoltaic Solar Energy Conference and Exhibition, Munich, Germany, 20–24 June 2016; Volume 53, pp. 2732–2734.
124. Faturrochman, G.J.J.; de Jong, M.M.M.; Santbergen, R.; Folkerts, W.; Zeman, M.; Smets, A.H.M.H.M. Maximizing Annual Yield of Bifacial Photovoltaic Noise Barriers. *Sol. Energy* **2018**, *162*, 300–305. [[CrossRef](#)]
125. Tina, G.M.; Scavo, F.B.; Aneli, S.; Gagliano, A. Assessment of the Electrical and Thermal Performances of Building Integrated Bifacial Photovoltaic Modules. *J. Clean. Prod.* **2021**, *313*, 127906. [[CrossRef](#)]
126. Attoye, D.E.; Hassan, A. A Review on Building Integrated Photovoltaic Façade Customization Potentials. *Sustainability* **2017**, *9*, 2287. [[CrossRef](#)]
127. Baumann, T.; Nussbaumer, H.; Klenk, M.; Dreisiebner, A.; Carigiet, F.; Baumgartner, F. Photovoltaic Systems with Vertically Mounted Bifacial PV Modules in Combination with Green Roofs. *Sol. Energy* **2019**, *190*, 139–146. [[CrossRef](#)]
128. Corfield, L. Photovoltaic Noise Barriers. Available online: <https://sunenergysite.eu/en/pvpowerplants/noisebarriers.php> (accessed on 15 July 2022).
129. Mishra, A. Delhi Metro To Install Bifacial Vertical Solar Panels. Available online: <https://swarajyamag.com/infrastructure/delhi-metro-to-install-bifacial-vertical-solar-panels> (accessed on 15 July 2022).